Food & Function

ROYAL SOCIETY OF CHEMISTRY

PAPER

View Article Online
View Journal | View Issue

Cite this: *Food Funct.*, 2026, **17**, 3186

Epigallocatechin-3-gallate ameliorates LPS-induced ARDS by modulating *Akkermansia*-associated SCFAs metabolism and inhibiting the JAK2/STAT3 candidate signaling pathway

Shiming Fan,†[a,b,c] Guofang Yin,†[a,c] Yan Ren,†[d] Xiaoqing Fan,[a,c] Yuling Liang,[a,c] Ning Ma,[c] Ying Luo,[e] Yi Deng,[b] Chunmei Zhang,[b] Tian Xiang,[f] Jing Zuo,[e] Jingli Tang,[g] Dan Luo*[a,c,h] and Xianming Fan *[a,c]

Acute respiratory distress syndrome (ARDS) is a leading cause of acute respiratory failure and mortality, characterized by significant inflammation and damage to the alveolar-capillary membrane, which disrupts gas exchange. Although the triggers of ARDS vary, uncontrolled inflammation plays a central role in its progression, with current treatment options being limited. Dysbiosis of the gut microbiota fuels systemic inflammation *via* the gut–lung axis and acts as a key driver of ARDS onset and progression. Epigallocatechin-3-gallate (EGCG), a major polyphenolic constituent derived from green tea, with known anti-inflammatory effects, and microbiota-modulating properties, holds potential as a therapeutic intervention for ARDS. This study investigated the mechanism of EGCG's intervention in ARDS and its impact on gut microbiota using C57BL/6J mice. The mice were divided into groups receiving different doses of EGCG pretreatment, followed by intratracheal instillation of lipopolysaccharide (LPS)-induced ARDS. Various techniques, including pathological examination, ELISA, and immunohistochemistry (IHC), were employed to assess pulmonary inflammation and examine intestinal tight junction integrity. Gut microbiota composition was analyzed *via* 16S rRNA sequencing. To further elucidate the role of the gut microbiota, fecal microbiota transplantation (FMT) was performed following gut microbiota depletion. Feces from EGCG-treated donor mice were transplanted into recipient mice, with results compared to the EGCG-pretreated group. A more focused investigation involved the transplantation of *Akkermansia muciniphila* (AKK), and its effects on pulmonary inflammation and intestinal tight-junction integrity were observed. Additionally, GC-MS analysis confirmed that AKK-derived metabolites were short-chain fatty acids (SCFAs), and the effects of SCFAs were compared to those of EGCG pretreatment. Network pharmacology and transcriptomic analysis suggested that SCFAs likely exert their effects through the JAK2/STAT3 signaling pathway. The effects of SCFAs and EGCG pretreatment were further validated using specific inhibitors to assess pulmonary and intestinal conditions. In the LPS-induced ARDS model, EGCG significantly reduced the inflammatory response, decreased inflammatory cell infiltration, and inhibited pro-inflammatory cytokine production, thereby limiting lung and intestinal tissue damage. Mechanistically, EGCG enriched the gut microbiota, particularly increasing AKK abundance, which promoted SCFAs production. These SCFAs entered systemic circulation, reached the lungs, and modulated the JAK2/STAT3 candidate signaling pathway to suppress inflammation, ultimately alleviating ARDS pathology. In conclusion, EGCG mitigates ARDS-related inflammatory damage by increasing *Akkermansia*

Received 10th December 2025,
Accepted 19th February 2026

DOI: 10.1039/d5fo05380c

rsc.li/food-function

[a]*Department of Respiratory and Critical Care Medicine, The Affiliated Hospital, Southwest Medical University, 646000 Luzhou, Sichuan, China. E-mail: fxm129@swmu.edu.cn, luodanwy1112@163.com; Tel: +86-13982769572, +86-15228283484*

[b]*Department of Respiratory and Critical Care Medicine, The People's Hospital of Jiang'anCounty, 644200 Yibin, Sichuan, China*

[c]*Inflammation & Allergic Diseases Research Unit, The Affiliated Hospital, Southwest Medical University, 646099 Luzhou, Sichuan, China*

[d]*Outpatient Department, Changning Hospital of Traditional Chinese Medicine, Yibin, Sichuan 644200, China*

[e]*Department of Respiratory and Critical Care Medicine, Jiang'an Hospital of Traditional Chinese Medicine, 644200 Yibin, Sichuan, China*

[f]*Department of Pathology, Changning Hospital of Traditional Chinese Medicine, Yibin, Sichuan 644200, China*

[g]*Department of Pediatrics, the People's Hospital of Jiang'an County, 644200 Yibin, Sichuan, China*

[h]*Laboratory Animal Centre, Model Animal and Human Disease Research of Luzhou Key Laboratory, Southwest Medical University, 646000 Luzhou, Sichuan, China*

† These authors contributed equally.

muciniphila abundance and enhancing SCFAs production, which inhibits the JAK2/STAT3 candidate pathway. This study introduces a novel gut microbiota-based approach for ARDS treatment and offers new insights into the role of gut-derived metabolites in ARDS pathogenesis.

1. Introduction

Acute respiratory distress syndrome (ARDS), a form of acute respiratory failure,[1] results from various triggers that initiate inflammatory cascades, oxidative stress, and vascular hyperpermeability.[2] These processes collectively disrupt the alveolar-capillary barrier, impair gas exchange, and compromise respiratory function.[3] Current clinical management emphasizes supportive strategies such as prone positioning, protective ventilation, and adjunctive therapies (*e.g.*, diuretics, hemofiltration, fluids, and vasopressors).[4] However, these approaches show limited efficacy in modulating the underlying inflammatory response or improving patient outcomes.[3,5] Critically, no existing drug specifically targets the molecular pathophysiology of ARDS to effectively suppress inflammation.[4]

Akkermansia muciniphila (AKK), a beneficial gut bacterium, alleviates systemic inflammation and preserves gut homeostasis.[6] Data from animal studies indicate that oral administration of AKK in LPS-induced ARDS models reduces pulmonary pro-inflammatory cytokines, decreases bronchoalveolar lavage fluid (BALF) inflammatory cell infiltration, and mitigates lung histopathology.[7,8] This protective effect likely arises from AKK's ability to repair intestinal barrier dysfunction, reduce bacteremia/endotoxemia, and modulate gut–lung immune crosstalk by polarizing macrophages toward an anti-inflammatory phenotype.[9,10] Notably, AKK's effects may be mediated through short-chain fatty acids (SCFAs, primarily acetate, propionate, and butyrate), which are produced by gut microbial fermentation.[11–13] In ARDS, SCFAs preserve mucosal integrity ("gut wall" effect) and exhibit dual immunomodulatory effects, including suppression of TNF-α/IL-6 and promotion of IL-10 secretion.[14] Experimental evidence supports that SCFA supplementation or SCFA-producing probiotics attenuate lung inflammation.[7,15,16] Critical unresolved questions include understanding the mechanistic relationship between AKK and SCFAs in regulating the gut–lung axis, particularly regarding how AKK orchestrates pulmonary immunity through SCFA-mediated pathways and identifying the specific downstream signaling effectors responsible for translating SCFA activity within the complex pathophysiological microenvironment of ARDS.

The Janus kinase 2/signal transducer and activator of transcription 3 (JAK2/STAT3) signaling pathway is essential for maintaining cellular homeostasis.[17] In ARDS models, multiple studies have shown that JAK2/STAT3 activation is significantly elevated, driving pulmonary inflammation, tissue damage, and respiratory failure.[18,19] Mechanistically, pathogenic stimuli (*e.g.*, LPS) activate JAK2/STAT3 in alveolar epithelial cells, triggering immune cell recruitment and pro-inflammatory cytokine release.[20] Emerging evidence links AKK to JAK2/STAT3 regulation. In inflammatory bowel disease (IBD) models, AKK supplementation reduces JAK2/p-STAT3 expression and inflammation, suggesting pathway modulation.[21,22] Similarly, SCFAs inhibit JAK2 phosphorylation and STAT3 nuclear translocation in colitis, attenuating inflammatory responses.[23–25] Despite these findings in other diseases, the coordination of JAK2/STAT3 signaling by AKK and SCFAs in ARDS remains unclear, necessitating further investigation into gut–lung crosstalk mechanisms.

EGCG, the principal catechin in green tea, exhibits potent antioxidant and anti-inflammatory activities.[26] Emerging evidence highlights its therapeutic potential in inflammatory diseases.[27] In ARDS models, EGCG intervention reduces pulmonary inflammatory cell infiltration, decreases lung wet/dry (W/D) ratios, and lowers pro-inflammatory cytokines in serum and BALF.[28,29] Notably, EGCG-rich diets significantly increase the relative abundance of AKK in the gut.[30] AKK elevation attenuates tissue inflammation, as demonstrated in IBD and neurodegenerative models.[31] Mechanistically, EGCG-induced AKK proliferation enhances SCFA production, which exerts systemic anti-inflammatory effects.[32] This suggests that EGCG may indirectly modulate inflammation *via* the AKK-SCFA axis. Furthermore, EGCG directly inhibits JAK2/STAT3 signaling. Across tumor, neuroinflammation, and dermatosis models, EGCG reduces JAK2/STAT3 phosphorylation and regulates pathway-related proteins.[33,34] It is hypothesized that EGCG could improve ARDS by enriching AKK, increasing SCFA production, and inhibiting the activation of the JAK2/STAT3 signaling pathway in the lungs. To validate this hypothesis, C57BL/6J mice were pretreated with EGCG before inducing ARDS with LPS, followed by multi-omics analyses of gut–lung axis crosstalk. The results revealed that EGCG treatment significantly increased the relative abundance of AKK in the gut, elevated SCFA levels, inhibited JAK2/STAT3 signaling activation in the lungs, and improved ARDS symptoms in mice. This study provides a comprehensive understanding of the mechanisms by which EGCG improves ARDS, offering a theoretical basis and potential targets for ARDS treatment strategies based on the gut–lung axis, with significant clinical translational value.

2. Materials and methods

2.1 Animal experiments and group allocation

Eight-week-old specific pathogen-free (SPF) male C57BL/6J mice, with an initial body weight of 24–26 g, were selected for this study. These mice were purchased from Chengdu Yaokang Biotechnology Co., Ltd, China, under the SCXK (Sichuan) 2020-034 license number. They were housed in individually ventilated cages with a density of five mice per cage, in the standard SPF animal facilities at Southwest Medical University.

The housing temperature was maintained ranging from 22 °C to 25 °C, and the relative humidity was maintained between 50% and 70%. A 12 h light/dark cycle was implemented, and the mice had free access to food and water. Ethical approval was obtained from Southwest Medical University (no. Swmu20240109), and all procedures adhered to the approved protocol and care guidelines. This study examined the effects of EGCG only during the initiation phase of inflammation under pre-treatment conditions; its therapeutic potential after inflammation is established remains to be validated before clinical translation.

The experimental design for Experiment 1 is shown in Fig. 1A. The mice were randomly assigned to four treatment groups (N = 8). Then, daily oral gavage was given; Control and LPS groups received PBS, while EGCG groups received PBS with EGCG. The LPS and LPS + EGCG (10 mg kg^{-1}, 20 mg kg^{-1}) groups received LPS intratracheally, while the Control group received PBS. Mice were anesthetized and euthanized for sample collection. Samples were collected aseptically under sterile conditions. Fecal samples were immediately stored at −80 °C. Blood samples were obtained *via* right-heart puncture, allowed to stand at room temperature for 2 h, and

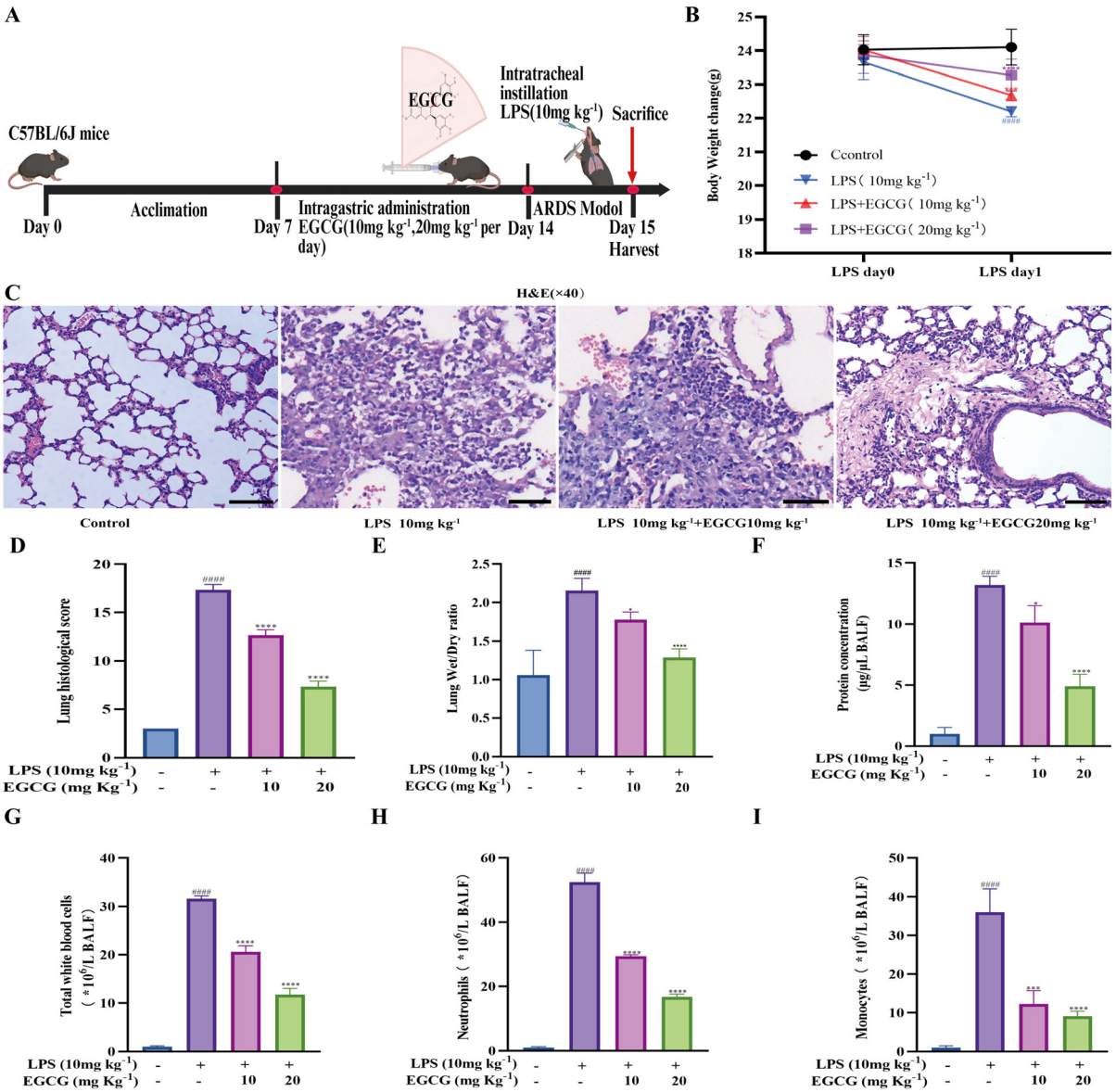

Fig. 1 EGCG ameliorates LPS-induced lung injury. (A) Experimental design schematic. (B) Body weight changes following treatment with LPS and EGCG. (C) H&E staining showing the histomorphological characteristics of the lung (scale bar = 50 μm). (D) Histological scores of lung tissues. (E) Wet-to-dry weight ratio of lung tissues. (F) Protein concentration in bronchoalveolar lavage fluid (BALF). (G–I) Cell counts in BALF, including total white blood cells, neutrophils, and mononuclear macrophages, measured using a hematology analyzer. All data are normalized to the control group. Data are presented as means ± SEMs (N = 8, $^{\#\#\#\#}p < 0.0001$, compared to the control group; $^{*}p < 0.05$, $^{***}p < 0.001$, $^{****}p < 0.001$, compared to the LPS-induced group).

then centrifuged at 1000*g* for 20 min at 4 °C. The serum was stored at −80 °C. Colon tissue was sectioned into 5 mm pieces from the middle part, rinsed with PBS, and fixed in either 10% formalin or 4% paraformaldehyde for histological analysis. The remaining colon tissue was rinsed with PBS, flash-frozen in liquid nitrogen, and stored at −80 °C. Lung tissue was processed in multiple ways. Some samples were fixed in the aforementioned fixatives for histological analysis. For bronchoalveolar lavage, the trachea and main bronchi were fully exposed, an incision was made in the trachea, and the trachea was lavaged three times with 1 mL of ice-cold saline to collect the bronchoalveolar lavage fluid (BALF). The BALF was centrifuged at 1500*g* for 10 min at 4 °C to separate the supernatant and cell pellet. Both the supernatant and the cell pellet were flash-frozen in liquid nitrogen and stored at −80 °C. Additionally, some intact lung tissue was added to RIPA lysis buffer or Trizol reagent containing inhibitors, flash-frozen in liquid nitrogen, and ground in a tissue grinder at 70 Hz for 1 minute, repeated ten times. The resulting liquid was stored at −80 °C for further molecular biological analysis.

The experimental design for Experiment 2 is shown in Fig. 5A. The mice were randomly and equally assigned to four groups (N = 8): the control group, the LPS group, the LPS + EGCG (20 mg kg^{-1}) group, and the LPS + EGCG feces group. For the LPS + EGCG (20 mg kg^{-1}) group, on the seventh day after EGCG administration, fecal samples were quickly collected and immediately stored at −80 °C for cryopreservation. The LPS + EGCG feces group received antibiotic (ABX) cocktail treatment, which involved daily oral gavage of vancomycin (100 mg kg^{-1}, cat. no. V301569-1 g), neomycin sulfate (200 mg kg^{-1}, cat. no. N109017-25 g), metronidazole (200 mg kg^{-1}, cat. no. M109874-25 g), and ampicillin (200 mg kg^{-1}, cat. no. A6265-5 g). Following the methodology of Hashimoto *et al.*,[3] fecal DNA was assayed from days 1 to 7. Fecal DNA quantity was nearly zero between days 5 and 7 (Fig. S4A), prompting the initiation of subsequent actions on day 7. Fecal matter from mice in the LPS + EGCG (20 mg kg^{-1}) group was homogenized with PBS at a concentration of 0.125 g mL^{-1}. After centrifugation at 600*g* for 5 min, the supernatant was collected and administered to mice in the LPS + EGCG feces group *via* daily intragastric gavage for 7 days. Throughout this period, fecal DNA concentration was measured daily from days 1 to 7, reaching the level of the LPS + EGCG (20 mg kg^{-1}) group by day 7 (Fig. S4B). Equal volumes of PBS were administered to the control, LPS, and LPS + EGCG (20 mg kg^{-1}) groups. Following the model construction approach in Experiment 1, LPS was intratracheally instilled into the LPS, LPS + EGCG (20 mg kg^{-1}), and LPS + EGCG feces groups, while an equal volume of PBS was instilled into the control group. Once the ARDS model was successfully established, blood, BALF, feces, lung tissue, and intestinal tissue were collected under sterile conditions and stored at −80 °C for subsequent analysis. Details and precautions regarding sample collection are presented in Experiment 1.

The experimental design for Experiment 3 is shown in Fig. 7A. The mice were randomly and evenly divided into four groups, (N = 8): the control group, the LPS group, the LPS + EGCG (20 mg kg^{-1}) group, and the LPS + AKK group. In the LPS + AKK group, mice were treated with an ABX cocktail, and fecal DNA was monitored from Day 1 to Day 7 following the protocol detailed in Experiment 2. The results revealed that fecal DNA content was nearly zero from Day 5 to Day 7 (Fig. S4C). Based on these findings, on Day 7, mice in this group were intragastrically administered AKK at a concentration of 2×10^9 cfu mL^{-1} for 7 consecutive days. During this period, fecal samples were collected daily, and AKK concentration in the feces was assessed using the AKK nucleic acid detection kit (Catalog No. BNCC 372727). By Day 6 and Day 7, the concentration of AKK in the feces of this group reached levels similar to those in the LPS + EGCG (20 mg kg^{-1}) group (Fig. S4D). On Day 7, following the model-building method from Experiment 1, LPS was intratracheally instilled into the mice in the LPS, LPS + EGCG (20 mg kg^{-1}), and LPS + AKK groups, while an equal volume of PBS was instilled into the control group. After successful model establishment, blood, BALF, lung tissue, and intestinal tissue samples were collected under strict aseptic conditions and stored at −80 °C for subsequent analysis. Sample collection was conducted in accordance with the procedures outlined in Experiment 1.

The experimental design for Experiment 4 is shown in Fig. 10A. The mice were randomly and evenly divided into four groups, (N = 8): the control group, the LPS group, the LPS + EGCG (20 mg kg^{-1}) group, and the LPS + SCFAs group. For the LPS + SCFAs group, as shown in Fig. 10A, mice received ABX cocktail therapy, and fecal DNA was monitored from Day 1 to Day 7 according to the protocol in Experiment 2. The results indicated that fecal DNA content was nearly zero from Day 5 onward (Fig. S4H). Based on this finding and previous studies, on Day 7, mice in this group were intragastrically administered sodium acetate (400 mg kg^{-1}), sodium propionate (100 mg kg^{-1}), and sodium butyrate (100 mg kg^{-1}). After intragastric administration, the content of SCFAs in the feces was measured using GC-MS. After 6–7 days of observation, the SCFAs content in the feces of this group was found to be similar to that in the LPS + EGCG (20 mg kg^{-1}) group (Fig. S4J–L). Following the model-building approach in Experiment 1, LPS was intratracheally instilled into the mice in the LPS, LPS + EGCG (20 mg kg^{-1}), and LPS + SCFAs groups, while an equal volume of PBS was instilled into the control group. Once the model was successfully established, blood, BALF, lung tissue, and intestinal tissue samples were collected under strict aseptic conditions and stored at −80 °C for subsequent analysis. The details and precautions for sample collection were carried out in accordance with the relevant procedures in Experiment 1.

The experimental design for Experiment 5 is shown in Fig. 13A. The mice were randomly and equally divided into five groups (N = 8): the control group, the LPS group, the LPS + EGCG (20 mg kg^{-1}) group, the LPS + SCFAs group, and the LPS + SCFAs + WP1066 group. The treatment procedures for the control, LPS, and LPS + EGCG (20 mg kg^{-1}) groups were consistent with those in Experiment 1. The treatment for the LPS

+ SCFAs group followed the method described in Experiment 4. The LPS + SCFAs + WP1066 group received intraperitoneal injections of WP1066 at a dose of 20 mg kg^{-1} twice a week (biweekly). Successful inhibition of the JAK2/STAT3 signaling pathway was confirmed by western blotting. The remaining treatments were identical to those in the LPS + SCFAs group. Subsequently, following the model-building protocol from Experiment 1, LPS was intratracheally instilled into the mice in the LPS-containing groups, while the control group received an equal volume of PBS. After the model was successfully established, blood, BALF, lung tissue, and intestinal tissue samples were collected under strict aseptic conditions and stored at −80 °C for subsequent analysis. All sample collection procedures were conducted in accordance with the relevant protocols from Experiment 1.

2.2 Histopathological examination and injury assessment

Following the research procedure outlined by Fan *et al.*,[35,36] tissues were fixed in 10% formalin, embedded in paraffin, and sectioned into 5 μm slices. The slices were dewaxed in xylene, hydrated in ethanol, and stained with hematoxylin and eosin (H&E). A high-resolution optical microscope (BX43, Olympus, Tokyo, Japan) was used for detailed histopathological examination. Lung tissue was assessed for interstitial and alveolar edema, hemorrhage, structural destruction, thickening of the alveolar septum, infiltration of inflammatory cells, formation of hyaline membranes, cell necrosis, dilation, and focal emphysema. Intestinal tissue was evaluated for mucosal edema, inflammation, epithelial hyperplasia, villous separation, and mucosal injury. Two pathologists performed double-blind scoring using the following criteria: 0 = no injury, 1 = mild injury, 2 = moderate injury, 3 = severe injury, and 4 = extremely severe histological changes.

2.3 Enzyme-linked immunosorbent assays (ELISA) and RNA extraction and Real-time polymerase chain reaction (RT-PCR) assay

Specific ELISA kits from Fine Biotech Co., Ltd (Wuhan, China) were used to quantify the levels of inflammatory factors, including IL-1β (Cat. No. EM0109), IL-6 (Cat. No. EM0121), TNF-α (Cat. No. EM0183), and SCFAs (Cat. No. EM2520) in serum, BALF, lung tissue, and feces. All experimental procedures were carried out in accordance with the manufacturer's instructions. Absorbance was measured at 450 nm using a Bio-Tek Synergy H1 Multi-Mode Microplate Reader.

The experimental procedure was adapted from Fan *et al.*[37] Total cellular RNA was extracted from lung and intestinal tissues using Trizol reagent according to the manufacturer's instructions. The extracted RNA was reverse-transcribed into cDNA using a reverse transcription kit (Bio-Rad Laboratories, California, USA, Cat. No. 1708891). RT-PCR was performed with the ABI 7500 prepstation (Applied Biosystems; Thermo Fisher Scientific, Inc.) and 2× M5 Hiper Realtime PCR Supermix (Cat. No. MF797-01). The primer sequences are provided in Table S1 of the SI. PCR conditions included initial denaturation at 95 °C for 1 min, followed by 40 cycles of denaturation at 95 °C for 15 seconds, annealing at 60 °C for 30 seconds, and extension at 72 °C for 45 seconds, with a final extension at 72 °C for 1 min. GAPDH from mice served as the internal control, and the $2^{-\Delta\Delta Ct}$ method was used to quantify the relative mRNA levels of inflammatory cytokines (IL-1β, IL-6, TNF-α), zonula occludens 1 (ZO-1), and occludin.

2.4 Extraction of fecal genomic DNA, sequencing of 16S rRNA gene, and microbiota data analysis

The experimental procedures in this study were based on the methodology outlined by Wu *et al.*[38] The preparation of fecal samples and the method for 16S rRNA sequencing were described previously.[39] In the present study, PCR amplification was performed using barcoded primers designed for the V3–V4 region of the 16S rRNA gene to amplify fecal DNA samples. Sequencing was carried out using the NovaSeq 6000 SP Reagent Kit V1.5 on the Illumina platform. Initially, quality control of the original sequences was performed using the Qubit® 2.0 Fluorometer (Thermo Scientific) according to preset default parameters. Bioinformatics analysis was then conducted using QIIME software (v1.9.0). Statistical analysis and graph creation were performed using programming languages such as R (3.6.0), Python (3.7.4), and Java to carry out α-diversity analysis, β-diversity analysis, microbial community clustering analysis, and differential species analysis.

2.5 Western blot analysis

The experimental procedures in this study were adapted from the description provided by Wang *et al.*[28] Whole lung tissue was weighed, mixed with 1 ml RIPA buffer, ground, and centrifuged to determine the protein concentration using a BCA kit. Equal amounts of protein underwent SDS-PAGE, were transferred to PVDF membranes, and blocked with 5% BSA. The primary antibodies used are listed in Table S2 and were incubated at 4 °C for 8–10 h. After washing with PBST, secondary antibodies, as detailed in Table S2, were applied, with incubation at 22 °C to 25 °C. Protein bands were visualized using an ECL kit, images were captured with the Tianneng system, and analyzed using ImageJ software.

2.6 Intestinal immunohistochemistry (IHC) and lung tissue immunofluorescence (IF)

IHC was performed following the methodology described by Jia *et al.*[40] Intestinal tissue specimens were embedded in paraffin, followed by deparaffinization, hydration, and blocking. Sections were incubated with primary antibodies (specific antibodies are listed in Table S2) at 4 °C for 8–10 h. After incubation with primary antibodies, the sections were incubated with a biotinylated secondary antibody (Cat. No. 21538-M) and SABC working solution. The expression of tight-junction proteins ZO-1 and occludin in intestinal tissue was observed using an optical microscope. The observed results were quantitatively analyzed using ImageJ software.

IF was performed according to the methodology specified by Yang *et al.*[41] Lung tissue sections were washed and blocked, then incubated with primary and secondary antibodies. The

sections were then incubated with a 5 μg mL^{-1} DAPI working solution for 5 minutes. Finally, sections were mounted with an anti-fade mounting medium, and images were captured using a fluorescence microscope.

2.7 Metabolomics and transcriptomics

Metabolomics was performed according to the methodology described by Fu *et al.*[42] Fecal samples from each mouse (20 mg) were weighed and mixed with 400 μL of a 70% methanol–water internal standard extraction solution. After vortex mixing and centrifugation, 200 μL of the supernatant was transferred for instrumental analysis. Chromatographic separation was conducted under T3 conditions using a Waters ACQUITY Premier HSS T3 Column (1.8 μm, 2.1 mm × 100 mm). Mobile phase A consisted of 0.1% formic acid in water, and mobile phase B contained 0.1% formic acid in acetonitrile. The column temperature was set to 40 °C, with a flow rate of 0.4 mL min^{-1} and an injection volume of 4 μL. Raw data were processed using the XCMS program combined with ProteoWizard software. Metabolites were identified *via* the metDNA method, and data analysis was performed using R language (version 4.1.2).

Transcriptomics was conducted following the procedure defined by Hu *et al.*[43] A 50 mg lung tissue sample was homogenized with 1 mL of TRIzol reagent at 4 °C. Total RNA was isolated and purified using the phenol–chloroform method. mRNA was then captured using Epi™ mRNA Capture Beads (cat. no. R2020-96), and library preparation was performed using the Epi™ mRNA Library Fast kit (cat. no. R1810). Library quality control was conducted with the Bioptic Qsep100 Analyzer (cat. no. R1809). Sequencing was performed on the NovaSeq high-throughput sequencing platform in PE150 mode.

2.8 Elucidation of the mechanism of EGCG in regulating the inflammatory response in ARDS using systematic network pharmacology methods

In this study, targets associated with EGCG were extracted from the Traditional Chinese Medicine Systems Pharmacology Database and Analysis Platform (TCMSP). The chemical structure of EGCG was retrieved in Simplified Molecular Input Line Entry System (SMILES) format from the PubChem database (https://pubchem.ncbi.nlm.nih.gov) (Fig. S5A). These SMILES strings were then entered into the SwissTargetPrediction small-molecule target prediction platform (https://www.swisstargetprediction.ch) to predict potential targets.

To construct a target library related to ARDS inflammation, the DisGeNET database (https://www.disgenet.org) was used, with search keywords such as "acute lung injury", "acute respiratory distress syndrome", "inflammation", and "sepsis". The GeneCards database (https://www.genecards.org) and the Online Mendelian Inheritance in Man database (OMIM, https://www.omim.org) were also searched using the same keywords, including "inflammatory" and related terms. The search results were filtered, with the screening criterion set to a GeneCards score of ≥3. The Venny v2.1.0 tool (https://bioinfogp.cnb.csic.es/tools/venny/index.html) was used to identify the common targets between the EGCG target gene database and the inflammation-related target library.

A protein–protein interaction (PPI) network was constructed using the STRING v12.0 database (https://string-db.org/), mapping EGCG targets to inflammation-related targets. Interaction data were exported in tab-separated values (TSV) format and imported into Cytoscape v3.10.1 for further analysis. Additionally, comprehensive gene annotation and analysis were performed using the web-based DAVID database (https://david.ncifcrf.gov/), with "Mus musculus" set as the pre-analysis species. Gene Ontology (GO) annotation and Kyoto Encyclopedia of Genes and Genomes (KEGG) pathway enrichment analysis were conducted. The GO analysis was categorized into three main domains: biological process (BP), cellular component (CC), and molecular function (MF). Finally, a bubble chart was generated using the free online bioinformatics data analysis resource at Bioinformatics (https://www.bioinformatics.com.cn).

2.9 Statistical analysis

Consistent results were ensured by replicating all experimental procedures, with each study repeated at least three times. Statistical analysis was performed using Tukey's multiple comparison test in GraphPad Prism Software (version 9.5.1; GraphPad Software, San Diego, CA) to determine significance between sample comparisons. Data are presented as Mean ± SEM, and statistical significance was set at $p < 0.05$.

3. Results

3.1 Protective effect of EGCG monotherapy against LPS-induced inflammation responses in ARDS mice

To comprehensively evaluate the anti-inflammatory effects of EGCG in LPS-induced ARDS, the safety profile of EGCG (≤20 mg kg^{-1}) was assessed through acute toxicity tests, including survival curves and body weight monitoring. Then, the ARDS model was optimized using a 10 mg kg^{-1} LPS intratracheal instillation based on survival outcomes and lung histopathological (H&E) analysis (Fig. S1). LPS-challenged mice exhibited significant weight loss and elevated lung W/D ratios at 24 h, compared to controls. Notably, EGCG pretreatment mitigated these changes (Fig. 1A, B and E). Additionally, EGCG attenuated LPS-induced pulmonary pathology, including edema, alveolar hemorrhage, inflammatory cell infiltration, hyaline membrane formation, alveolar thickening, and epithelial necrosis, resulting in reduced histopathological scores (Fig. 1C and D). Furthermore, EGCG suppressed LPS-driven increases in BALF protein concentration and inflammatory cell counts (Fig. 1F–I). Critically, EGCG pretreatment downregulated the expression and secretion of IL-1β, IL-6, and TNF-α in lung tissue, with the 20 mg kg^{-1} EGCG dose showing the most significant effect (Fig. 2A–L). In conclusion, this study demonstrates that EGCG (20 mg kg^{-1}) effectively alleviates LPS-induced ARDS by reducing inflammation and tissue damage in mice.

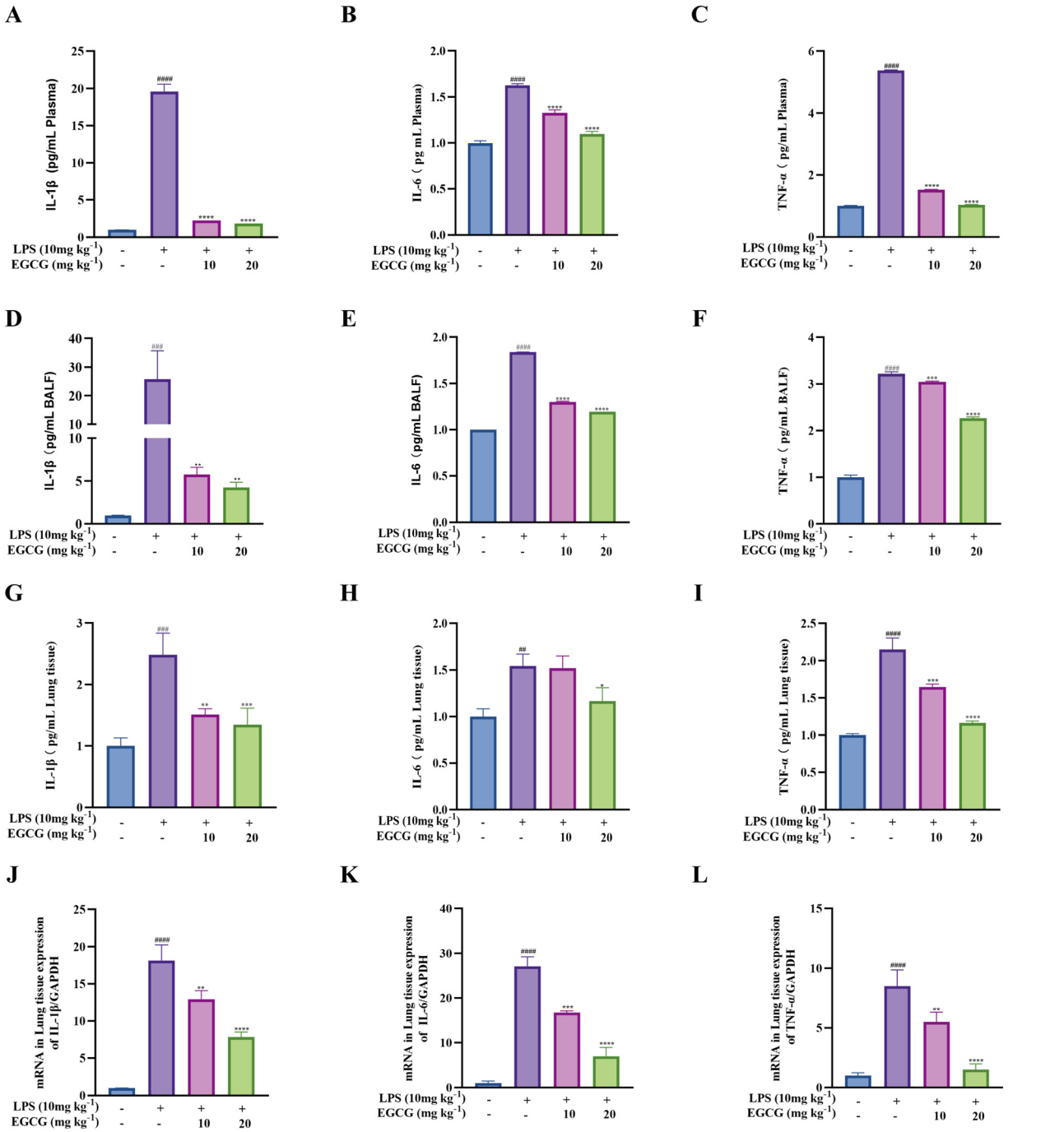

Fig. 2 EGCG ameliorates LPS-induced inflammation. (A–C) Serum levels of inflammatory factors (IL-1β, IL-6, TNF-α) measured using ELISA. (D–F) Inflammatory factor levels (IL-1β, IL-6, TNF-α) in BALF measured using ELISA. (G–I) Inflammatory factor levels (IL-1β, IL-6, TNF-α) in lung tissue, determined by ELISA. (J–L) mRNA expression of IL-1β, IL-6, and TNF-α in lung tissue assessed by RT-PCR. Data are normalized to the control group and presented as means ± SEMs (N = 8, $^{\#\#}p < 0.01$, $^{\#\#\#}p < 0.001$, $^{\#\#\#\#}p < 0.0001$, compared to the control group; $^{*}p < 0.05$, $^{**}p < 0.01$, $^{***}p < 0.001$, $^{****}p < 0.0001$, compared to the LPS-induced group).

3.2 Gut microbiota remodeling by EGCG mediates protection against LPS-triggered ARDS

The gut microbiota, a key regulator of host immunity *via* the gut–lung axis, plays a significant role in the inflammatory injury associated with ARDS. While EGCG is known to modulate gut microbiota,[44] its therapeutic efficacy in alleviating ARDS inflammation through this specific mechanism remains to be further explored. To address this, 16S rRNA sequencing was employed to analyze fecal samples. Venn diagrams, α-diversity metrics (Chao index, ACE index, observed features, Shannon diversity index, and Simpson diversity index), and

β-diversity analysis revealed that while the microbial community compositions of the EGCG-treated, LPS, and control groups were similar both statistically and biologically, distinct microbial taxa were identified in the EGCG-treated group (Fig. S2). At the phylum, family, genus, and species levels, the relative abundance of specific microbial taxa in the EGCG-treated group, calculated as a percentage of intestinal bacteria, exhibited dynamic changes compared to the LPS and control groups. Notably, the relative abundance of beneficial bacteria within the phylum Verrucomicrobia showed a significant increase (Fig. S3 and Fig. 3A). Linear discriminant analysis effect size (LEfSe) further demonstrated that the relative abundance of AKK was significantly higher in the EGCG treatment group compared to the LPS and control groups (Fig. 3B).

Previous studies have shown that LPS-induced inflammation in ARDS leads to intestinal pathology, including mucosal edema, inflammatory cell infiltration, and disruption of tight-junction proteins, ultimately compromising intestinal barrier function and facilitating the translocation of pathogenic mediators into systemic circulation.[45] As a potent antioxidant, EGCG may help preserve intestinal homeostasis by mitigating these effects.[46] In line with this, our histopathological analysis revealed that LPS challenge caused severe intestinal damage, including mucosal swelling, villus separation, and leukocyte

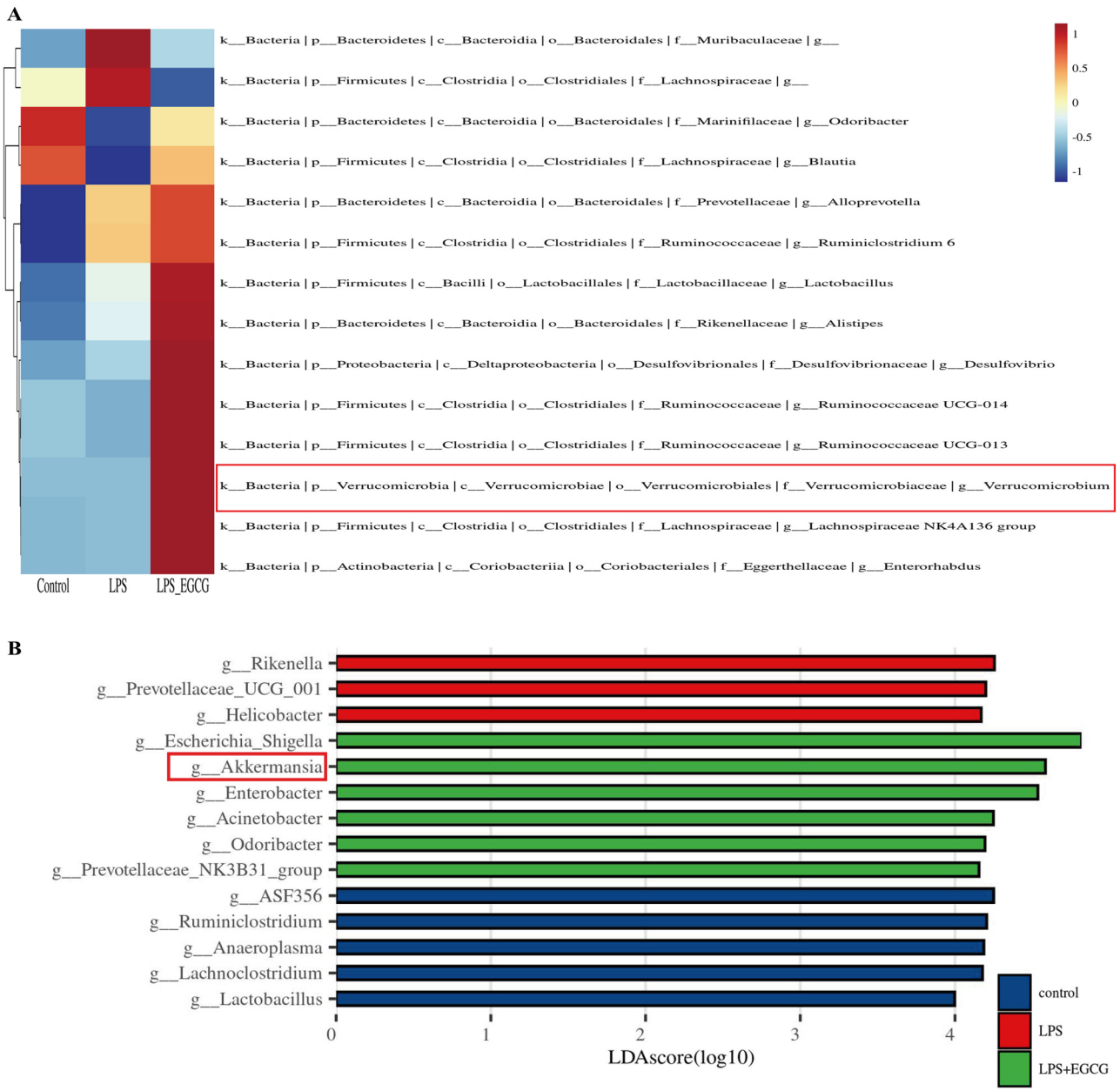

Fig. 3 Administration of EGCG alters gut microbial composition in mice. (A) Community heatmap analysis at the genus level. (B) LEfSe analysis of differentially abundant taxa detected among different groups after treatment with EGCG and LPS (N = 5).

aggregation, whereas EGCG pretreatment significantly alleviated these pathological changes (Fig. 4A and B). RT-PCR and western blot analysis demonstrated that LPS downregulated the expression of ZO-1 and occludin in colon tissue, but EGCG pretreatment (with the 20 mg kg^{-1} dose showing maximal efficacy) reversed this effect (Fig. 4C–G). IHC further confirmed these protein expression patterns (Fig. 4H–J). These results suggest that EGCG may alleviate LPS-induced ARDS by modulating the intestinal microecological environment, with *Akkermansia muciniphila* (AKK) potentially playing a key role.

3.3 Fecal microbiota transplantation reveals EGCG's role in alleviating ARDS through gut microbiota regulation and AKK enrichment

To further elucidate the mechanism by which EGCG modulates the inflammatory response in ARDS mice through gut microbiota, a fecal microbiota transplantation (FMT) experiment was conducted (Fig. 5A). Protein analysis revealed that the protein concentration in the BALF of mice receiving EGCG-FMT was significantly lower than in the LPS group and comparable to that in the LPS + EGCG (20 mg kg^{-1}) group (Fig. 5B). Lung damage, inflammatory cell infiltration, and pro-inflammatory cytokine levels in serum, BALF, and lung tissue showed consistent trends with the observed changes in BALF protein levels (Fig. 5C–S). In the gut, EGCG-FMT mice exhibited reduced intestinal inflammatory pathology compared to the LPS group, with histopathological scores similar to those in the LPS + EGCG group (Fig. 6A and B). Moreover, the mRNA and protein expression of ZO-1 and occludin in the colon were restored in EGCG-FMT mice, showing no significant difference from the LPS + EGCG group (Fig. 6C–G). Gut microbiota analysis in EGCG-FMT mice post-LPS treatment, alongside control and LPS groups, revealed distinct community composition through beta-diversity analysis (Fig. 6H). Unique taxonomic features at the genus and species levels were observed in EGCG-FMT mice, with a significantly higher relative abundance of AKK compared to the control and LPS groups (Fig. 6I and J). In summary, EGCG-modulated gut microbiota may mitigate LPS-induced ARDS inflammatory damage independently, potentially linked to AKK enrichment and enhanced intestinal barrier function.

3.4 AKK as key mediator of EGCG's anti-inflammatory effects in LPS-induced ARDS mice

Both EGCG and EGCG-FMT treatments significantly increased the abundance of AKK. Based on these findings, AKK plays a key role in regulating the host's inflammatory response to LPS-induced ARDS. To test this hypothesis, AKK was transplanted into mice, and the results showed that, compared to the LPS group, the protein levels in BALF from AKK-transplanted mice were significantly reduced, reaching levels comparable to those of the LPS + EGCG (20 mg kg^{-1}) group (Fig. 7A and B). Importantly, the severity of lung pathology, inflammatory cell infiltration, and pro-inflammatory cytokine levels in serum, BALF, and lung tissue consistently mirrored the changes in BALF protein concentrations (Fig. 7C–S). In the intestine, AKK transplantation significantly alleviated LPS-induced inflammatory damage, with histological scores comparable to those of the LPS + EGCG group (Fig. 8A and B). Furthermore, AKK transplantation restored the mRNA and protein expression of tight junction proteins (ZO-1 and occludin) in the colon to levels similar to those observed in the LPS + EGCG group (Fig. 8C–G). Collectively, these results demonstrate that AKK alone is sufficient to mitigate LPS-induced ARDS inflammation, with efficacy comparable to EGCG treatment. These results strongly support the conclusion that EGCG alleviates ARDS primarily by enriching the relative abundance of AKK, thereby enhancing gut barrier integrity and promoting systemic anti-inflammatory responses.

3.5 EGCG ameliorates ARDS through AKK-mediated SCFAs production and gut–lung axis modulation

To identify the key mediators underlying AKK's inhibitory effects on ARDS inflammation, metabolomic profiling of treatment-associated metabolites was performed. Principal component analysis (PCA) revealed distinct fecal metabolite profiles in the LPS + AKK group compared to both control and LPS groups (Fig. 9A). Targeted analysis identified SCFAs as the most significantly altered anti-inflammatory metabolites (Fig. 9B). GC-MS analysis showed that compared with the LPS group, the levels of key SCFA components—acetic acid, propionic acid, and butyric acid—in feces, serum, and lung tissues all exhibited an upward trend in mice treated with EGCG and AKK. Notably, no statistically significant difference was observed between the LPS + AKK group and the LPS + EGCG 20 mg kg^{-1} group (Fig. 9C–K). Previous studies have reported that SCFAs content can be measured using an ELISA kit.[47] Using the ELISA kit for detection, the present study observed that the trends in SCFAs content in feces, serum, and lung tissues were highly consistent with the results from GC-MS analysis (Fig. S4E–G). Subsequently, GC-MS analysis was conducted on mice treated with AKK. The results revealed that acetic acid, propionic acid, and butyric acid together accounted for 98% of the total SCFAs, with an approximate molar ratio of 4 : 1 : 1 (Fig. S4I). These results strongly support the mechanistic model that EGCG induces SCFA production, which enters the systemic circulation and accumulates in lung tissues. In the lung, SCFAs' main components (acetate, propionate, and butyrate) act synergistically to alleviate the inflammatory response in ARDS.

To verify this model, SCFAs were administered to mice, which were then challenged with LPS (Fig. 10A). Protein content in the BALF of mice in the LPS + SCFAs group was significantly lower compared to the LPS group, with no statistically significant difference when compared to the LPS + EGCG 20 mg kg^{-1} group (Fig. 10B). Therapeutic effects were observed across multiple parameters: lung pathology and inflammatory cell infiltration showed marked improvement, while pro-inflammatory cytokine levels in serum, BALF, and lung tissue were significantly reduced (Fig. 10C–S). Additionally, intestinal barrier integrity was restored, as evidenced by improved histopathological scores and upregulation of tight junction proteins

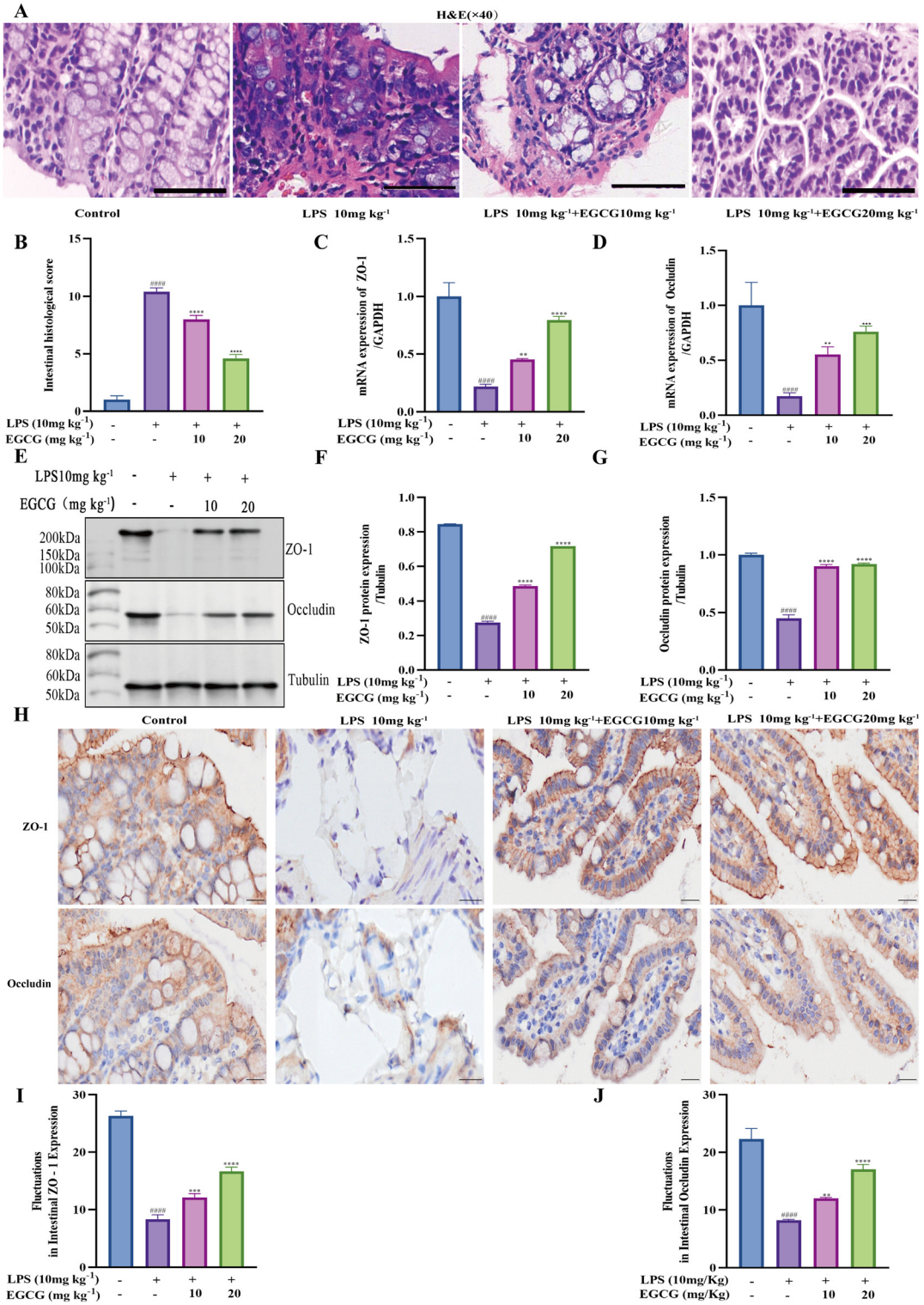

Fig. 4 EGCG ameliorates LPS-induced intestinal mucosal injury. (A) H&E staining of intestinal tissues from each group of mice (scale bar = 50 μm). (B) Quantitative analysis of histological scores of intestinal tissues. (C and D) RT-PCR analysis of ZO-1 and occludin levels in mouse intestinal tissues. (E) Western blot detection of ZO-1 and occludin protein expression in intestinal tissues. (F and G) Relative protein expression levels of ZO-1 and occludin normalized to tubulin, measured using ImageJ software. (H) Immunohistochemistry of ZO-1 and occludin protein expression in mouse intestinal tissues (scale bar = 20 μm). (I and J) Mean Fluorescence Intensity (MFI) of ZO-1 and occludin proteins detected by ImageJ. All data were normalized to the control group. Data are presented as means ± SEMs (N = 8, $^{\#\#\#\#}p < 0.0001$ compared to the control group; $^{**}p < 0.01$, $^{***}p < 0.001$, $^{****}p < 0.0001$ compared to the LPS-induced group).

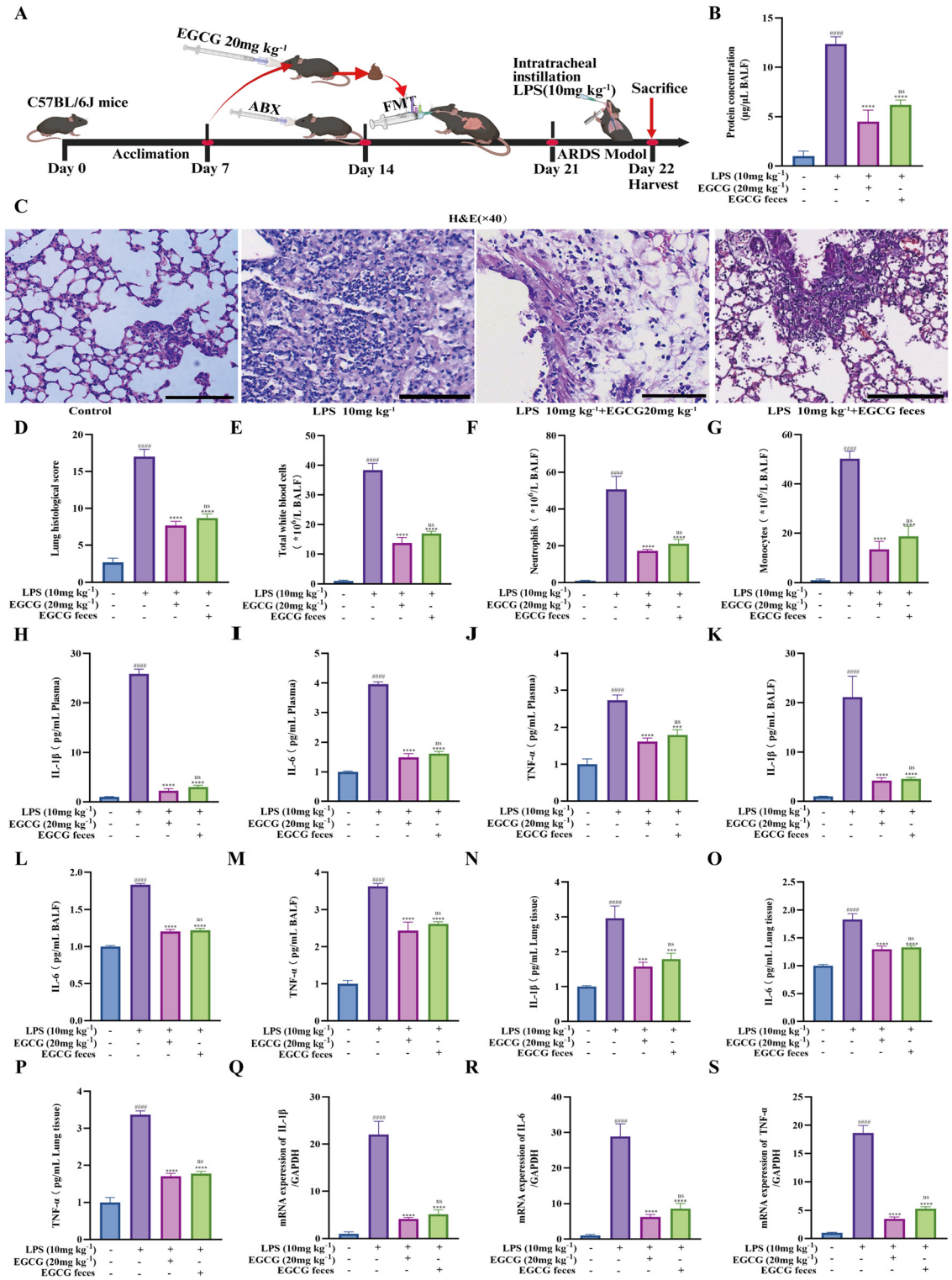

Fig. 5 Gut microbiota from EGCG-treated mice alleviates LPS-induced inflammation and lung injury. (A) Experimental design diagram for Experiment 2. Antibiotic cocktail treatment (ABX). (B) Protein concentration in BALF. (C) H&E staining reveals histomorphological characteristics of lung tissues (scale bar = 50 μm). (D) Histological scores of lung tissues, enabling quantitative analysis. (E–G) Hematology analyzer-based cell count, including total white blood cells, neutrophils, and mononuclear macrophages. (H–J) Measurement of inflammatory factors (IL-1β, IL-6, and TNF-α) in serum using ELISA kits. (K–M) Measurement of inflammatory factors (IL-1β, IL-6, and TNF-α) in BALF using ELISA kits. (N–P) ELISA analysis of inflammatory factors (IL-1β, IL-6, TNF-α) in lung tissues. (Q–S) RT-PCR measurement of inflammatory factors (IL-1β, IL-6, TNF-α) in lung tissues. All data were normalized to the control group. Data are presented as means ± SEMs (N = 8, $^{\#\#\#\#}p < 0.0001$, compared to the control group; $^{****}p < 0.0001$, compared to the LPS-induced group; $^{ns}p > 0.05$, compared to the LPS + EGCG 20 mg kg^{-1} group).

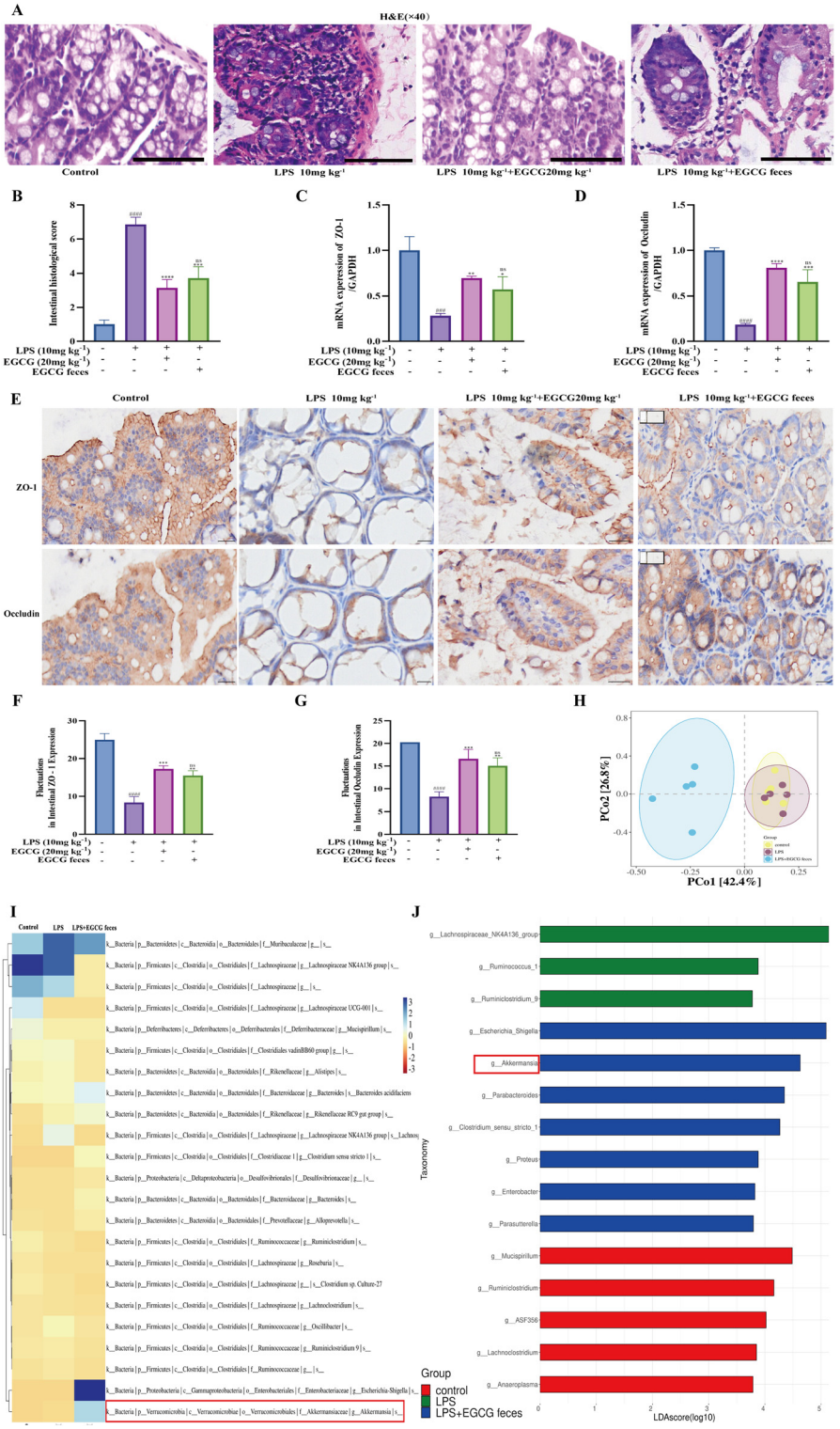

Fig. 6 Gut microbiota from EGCG-treated mice alleviates LPS-induced intestinal mucosal injury. (A) H&E staining of intestinal tissues from each group of mice (scale bar = 50 μm). (B) Quantitative analysis of histological scores of intestinal tissues. (C and D) RT-PCR analysis of ZO-1 and occludin levels in mouse intestinal tissues. (E) Immunohistochemical detection of ZO-1 and occludin protein expression in intestinal tissues (scale bar = 20 μm). (F and G) Mean Fluorescence Intensity (MFI) of ZO-1 and occludin proteins measured by ImageJ. (H) β-Diversity analysis of gut microbiota in different experimental groups based on principal coordinate analysis (PCoA) (N = 5). (I) Community heatmap analysis at the species level. (J) LEfSe analysis of differentially abundant taxa among experimental groups. All data were normalized to the control group. Data are presented as means ± SEMs (N = 8, $^{\#\#\#\#}p < 0.0001$ compared to the control group; $^{**}p < 0.01$, $^{***}p < 0.001$, $^{****}p < 0.0001$ compared to the LPS-induced group; $^{ns}p > 0.05$ compared to the LPS + EGCG 20 mg kg^{-1} group).

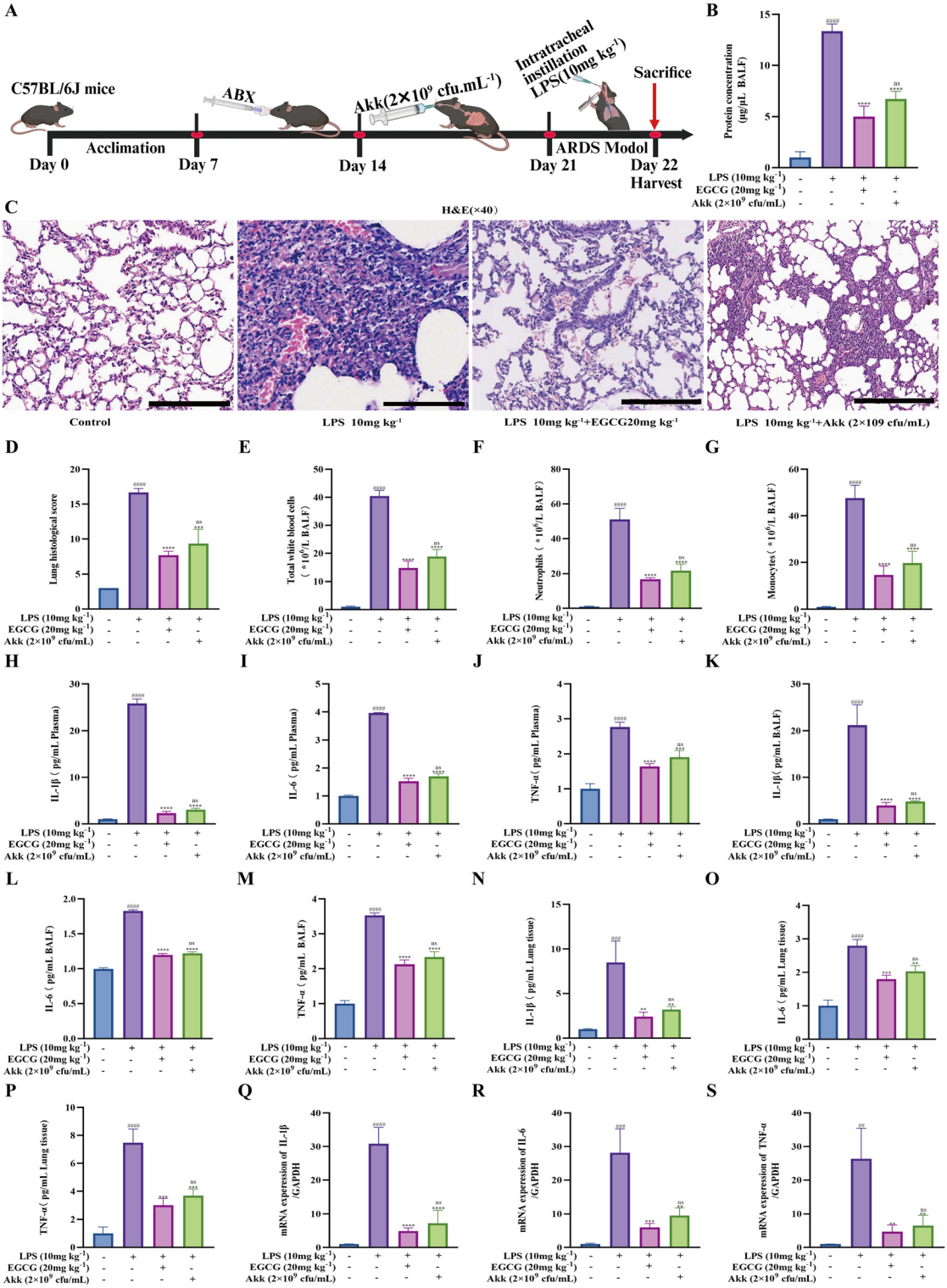

Fig. 7 AKK alleviates LPS-induced inflammation and lung injury. (A) Diagram illustrating the experimental design employed in Experiment 3. (B) Protein concentration in BALF. (C) H&E staining reveals histomorphological characteristics of the lung (scale bar = 50 μm). (D) Histological scores of lung tissues, enabling quantitative analysis. (E–G) Hematology analyzer-based cell count of total white blood cells, neutrophils, and mononuclear macrophages. (H–J) Levels of inflammatory factors (IL-1β, IL-6, TNF-α) in serum measured using ELISA kits. (K–M) Measurement of inflammatory factors (IL-1β, IL-6, TNF-α) in BALF using ELISA kits. (N–P) ELISA analysis of inflammatory factors (IL-1β, IL-6, TNF-α) in lung tissues. (Q–S) RT-PCR analysis of inflammatory factors (IL-1β, IL-6, TNF-α) in lung tissues. All data were normalized to the control group. Data are presented as means ± SEMs (N = 8, $^{\#\#\#}p < 0.001$, $^{\#\#\#\#}p < 0.0001$ compared to the control group; $^{**}p < 0.01$, $^{***}p < 0.001$, $^{****}p < 0.0001$ compared to the LPS-induced group; $^{ns}p > 0.05$ compared to the LPS + EGCG 20 mg kg^{-1} group).

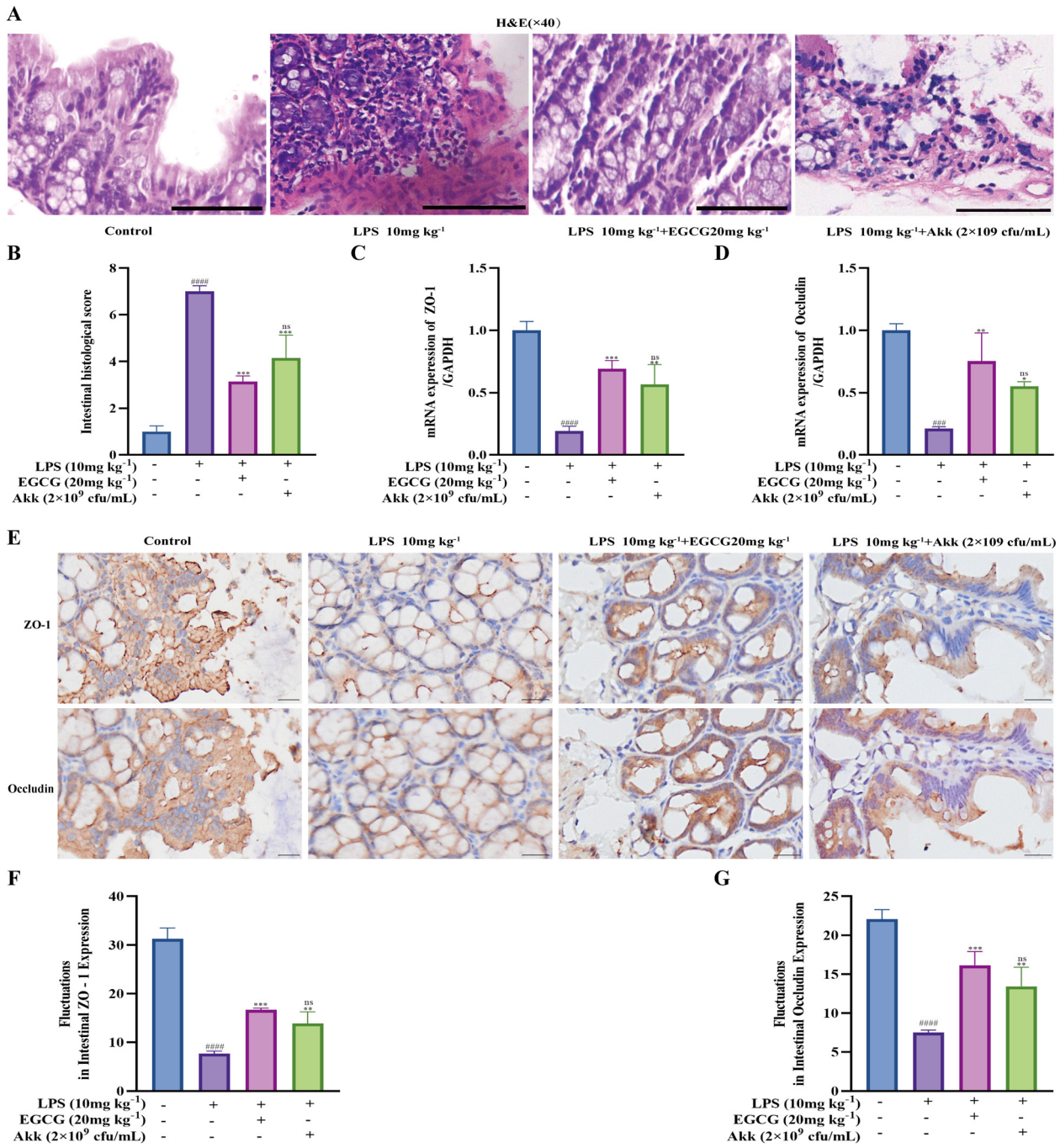

Fig. 8 AKK alleviates LPS-induced intestinal mucosal injury. (A) H&E staining of intestinal tissues from each group of mice (scale bar = 50 μm). (B) Quantitative analysis of histological scores of intestinal tissues. (C and D) RT-PCR analysis of ZO-1 and occludin levels in mouse intestinal tissues. (E) Immunohistochemical detection of ZO-1 and occludin protein expression in intestinal tissues (scale bar = 20 μm). (F and G) Mean Fluorescence Intensity (MFI) of ZO-1 and occludin proteins measured by ImageJ. All data were normalized to the control group. Data are presented as means ± SEMs (N = 8, $^{\#\#\#}p < 0.001$, $^{\#\#\#\#}p < 0.0001$ compared to the control group; $^{*}p < 0.05$, $^{**}p < 0.01$, $^{***}p < 0.001$ compared to the LPS-induced group; $^{ns}p > 0.05$ compared to the LPS + EGCG 20 mg kg^{-1} group).

ZO-1 and occludin (Fig. 11A–G). Collectively, these results demonstrate that SCFAs alone can replicate EGCG's protective effects against LPS-induced ARDS, strongly suggesting that EGCG exerts its anti-inflammatory action primarily through SCFA elevation.

3.6 SCFAs alleviate LPS-induced pulmonary and intestinal Injury in ARDS *via* the JAK2/STAT3 signaling pathway

To elucidate the mechanism by which SCFAs mitigate inflammatory injury in ARDS, network pharmacology and transcrip-

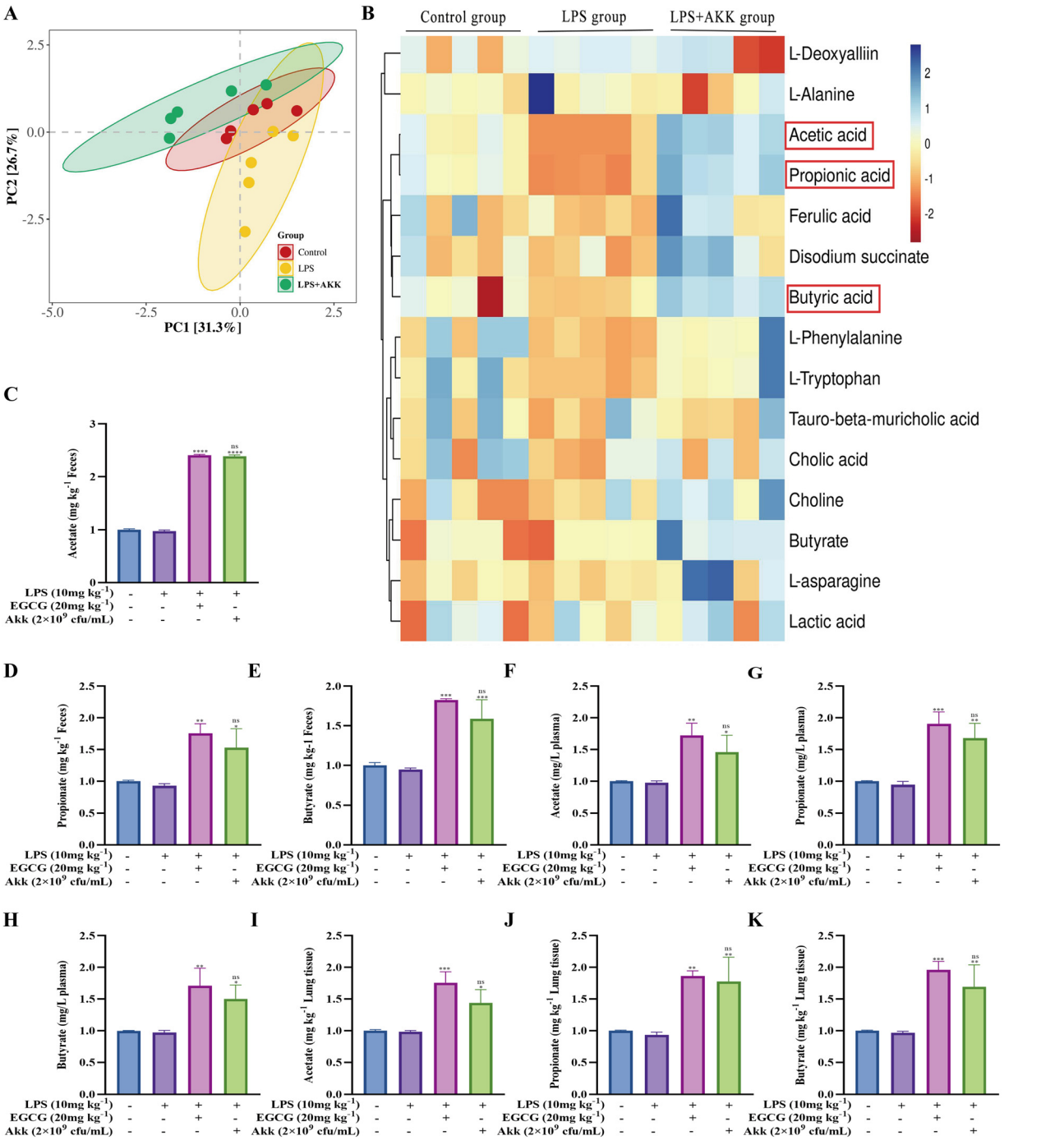

Fig. 9 AKK exerts its effects by increasing the concentration of SCFAs. (A) Analysis of metabolites in mice treated with LPS and/or AKK based on principal component analysis (PCA). (B) Heatmap analysis of fecal metabolites. The concentrations of acetate (C), propionate (D), and butyrate (E) in feces were measured by gas chromatography-mass spectrometry (GC-MS). The concentrations of acetate (F), propionate (G), and butyrate (H) in blood were measured by GC-MS. The concentrations of acetate (I), propionate (J), and butyrate (K) in lung tissue were measured by GC-MS. All data were normalized to the control group. Data are presented as means ± SEMs (N = 8, *p < 0.05, **p < 0.01, ***p < 0.001, ****p < 0.0001 compared to the LPS-induced group; ^{ns}p > 0.05 compared to the LPS + EGCG 20 mg kg^{-1} group).

tomics analyses were integrated. Network pharmacology identified 96 overlapping genes between EGCG target genes and ARDS-related genes (Fig. S5B). Transcriptomics further identified 30 differentially expressed genes shared across the control, LPS, and LPS + SCFAs groups, which also overlapped with ARDS targets (Fig. S5C). These datasets were combined to construct a protein–protein interaction (PPI) network using STRING and Cytoscape, identifying JAK2 and STAT3 as hub genes in anti-inflammatory pathways (Fig. S5D and E). MetaScape enrichment analysis linked the overlapping genes

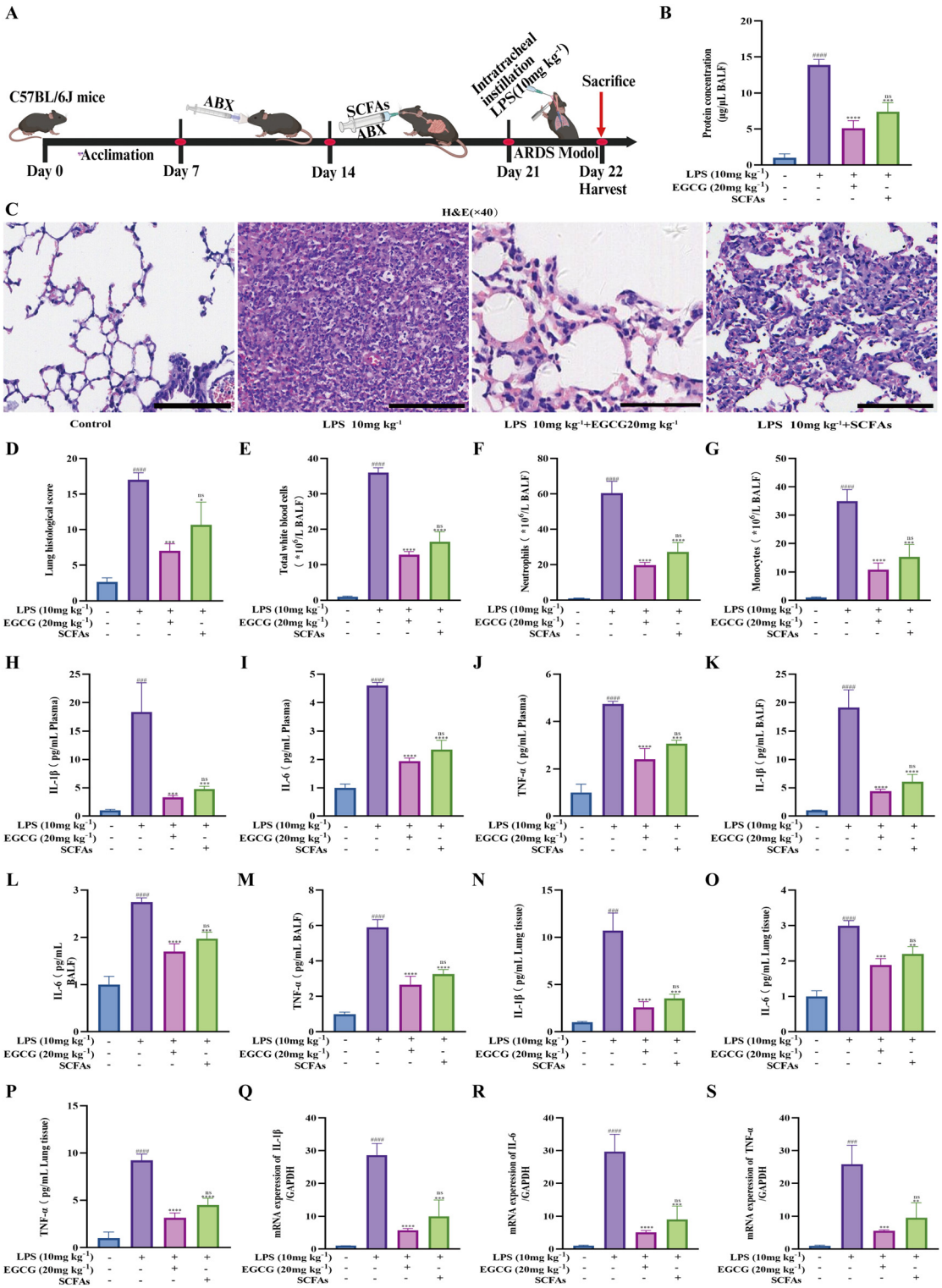

Fig. 10 SCFAs alleviate LPS-induced lung injury and inflammation. (A) Diagram illustrating the experimental design employed in Experiment 4. (B) Protein concentration in BALF. (C) H&E staining revealing histomorphological characteristics of the lung (scale bar = 50 μm). (D) Histological scores of lung tissues enabling quantitative analysis. (E–G) Hematology analyzer-based cell count of total white blood cells, neutrophils, and mononuclear macrophages. (H–J) Measurement of inflammatory factors (IL-1β, IL-6, and TNF-α) in serum using ELISA kits. (K–M) Measurement of inflammatory factors (IL-1β, IL-6, and TNF-α) in BALF using ELISA kits. (N–P) ELISA analysis of inflammatory factors (IL-1β, IL-6, TNF-α) in lung tissues. (Q–S) RT-PCR analysis of inflammatory factors (IL-1β, IL-6, TNF-α) in lung tissues. All data were normalized to the control group. Data are presented as means ± SEMs (N = 8, $^{\#\#\#}p < 0.001$, $^{\#\#\#\#}p < 0.0001$, compared to the control group; $^{*}p < 0.05$, $^{**}p < 0.01$, $^{***}p < 0.001$, $^{****}p < 0.0001$, compared to the LPS-induced group; $^{ns}p > 0.05$, compared to the LPS + EGCG 20 mg kg^{-1} group).

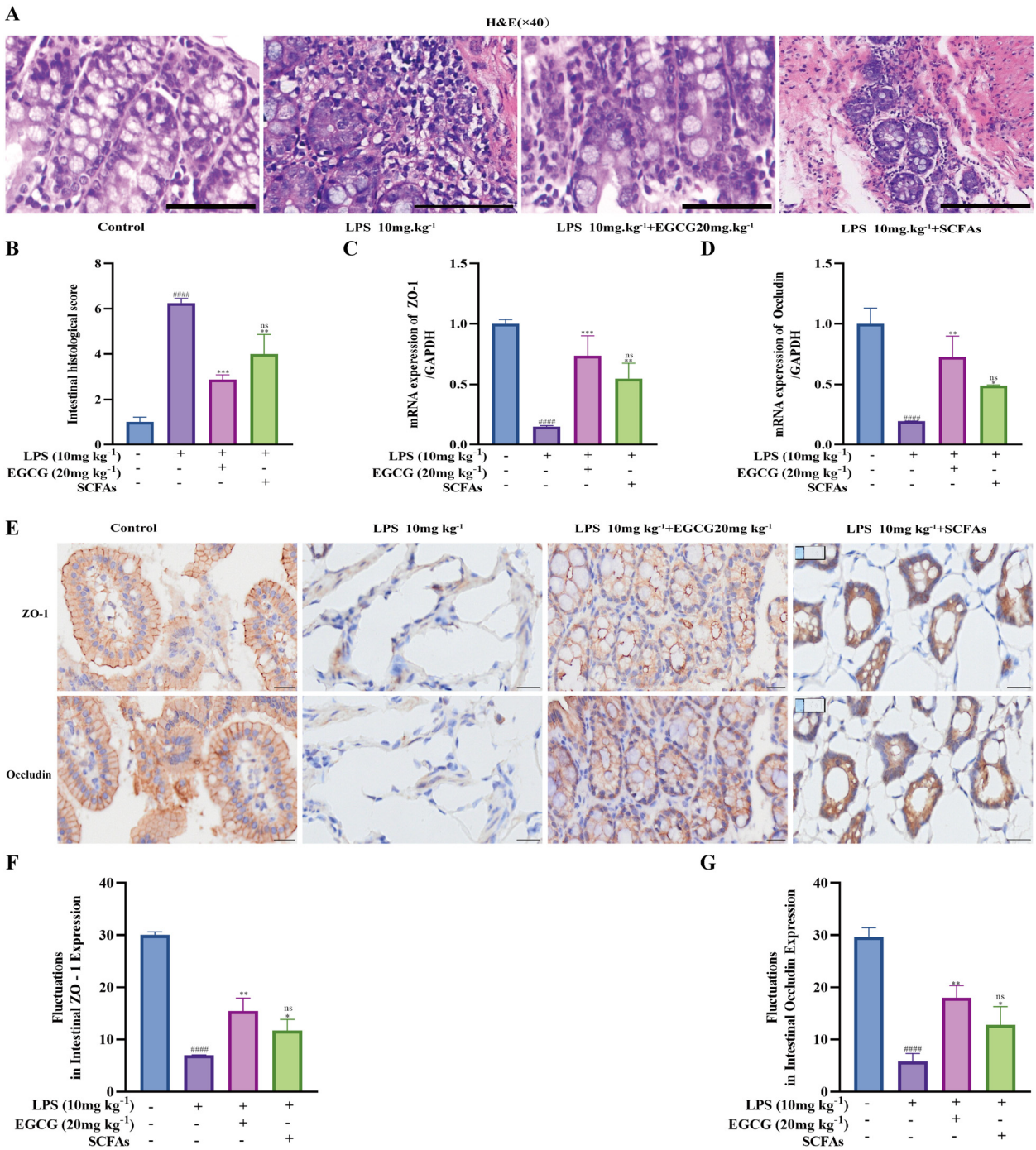

Fig. 11 SCFAs alleviate LPS-induced intestinal mucosal injury. (A) H&E staining of intestinal tissues from each group of mice (scale bar = 50 μm). (B) Quantitative analysis of histological scores of intestinal tissues. (C and D) RT-PCR analysis of ZO-1 and occludin levels in mouse intestinal tissues. (E) Immunohistochemical detection of ZO-1 and occludin protein expression in intestinal tissues (scale bar = 20 μm). (F and G) Mean Fluorescence Intensity (MFI) of ZO-1 and occludin proteins measured by ImageJ. All data were normalized to the control group. Data are presented as means ± SEMs (N = 8, $^{\#\#\#\#}p < 0.0001$, compared to the control group; $^{*}p < 0.05$, $^{**}p < 0.01$, $^{***}p < 0.001$, compared to the LPS-induced group; $^{ns}p > 0.05$, compared to the LPS + EGCG 20 mg kg^{-1} group).

to inflammation-related biological processes and pathways (Fig. S6). KEGG analysis highlighted the JAK/STAT, NF-κB, MAPK, PI3K/AKT/HIF-α, and Wnt pathways as important mediators of SCFAs' effects (Fig. 12A and B).

To clarify the regulatory mechanism, the protein expression of key inflammatory effectors was analyzed. western blot analysis showed that LPS stimulation significantly increased the phosphorylation levels of JAK2 and STAT3, whereas pretreat-

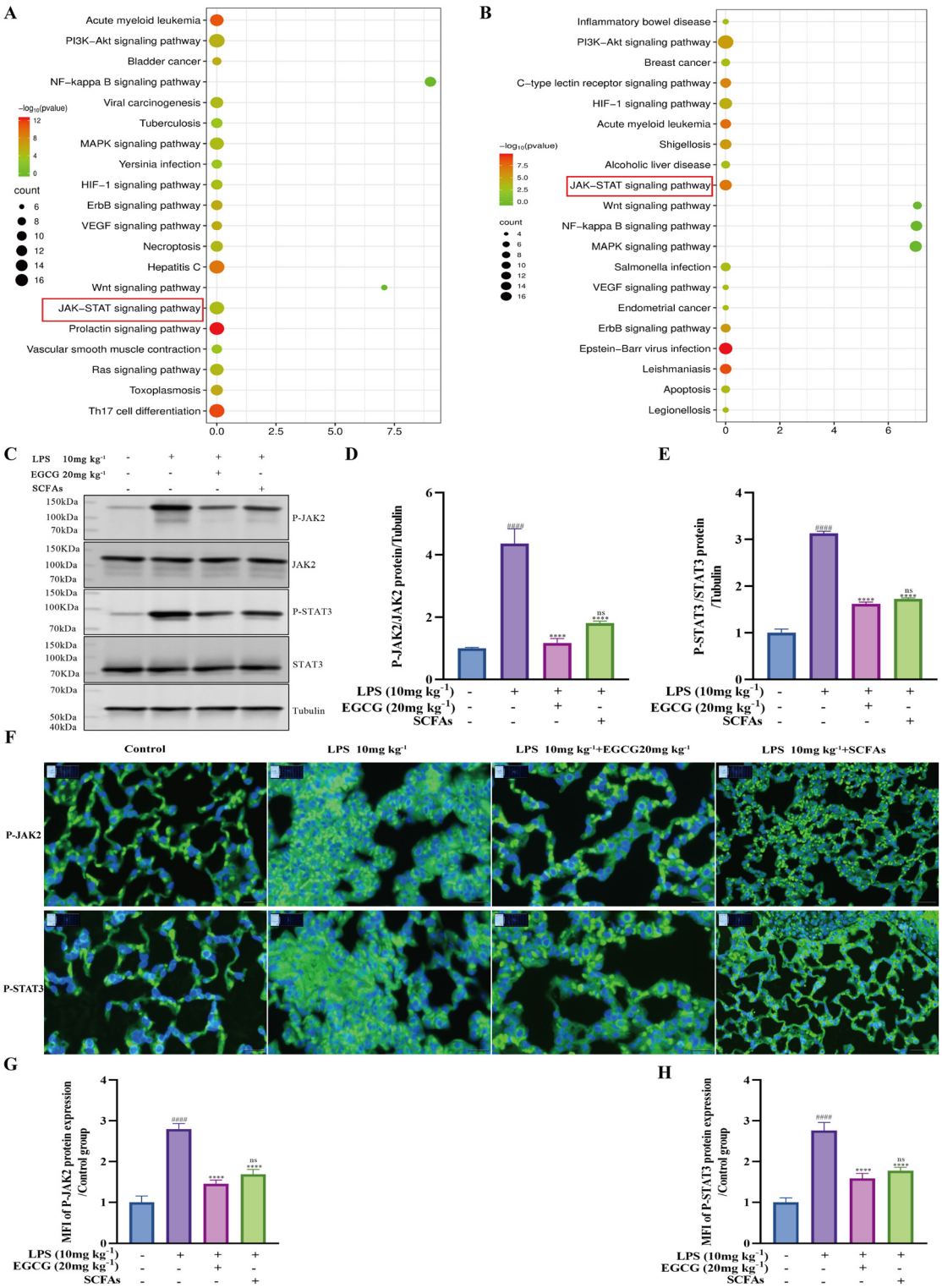

Fig. 12 JAK2/STAT3 is the target of SCFA action. (A) KEGG pathway enrichment analysis of overlapping genes in network pharmacology. (B) KEGG pathway enrichment analysis of overlapping genes in transcriptomics. (C) Protein expression levels of P-JAK2, JAK2, P-STAT3, and STAT3 in lung tissues from mice in each group, detected by western blot analysis. (D and E) Relative protein expression levels of P-JAK2/JAK2 and P-STAT3/STAT3 to Tubulin, measured using ImageJ software. (F) Immunofluorescence detection of P-JAK2 and P-STAT3 protein expression in lung tissues from mice in each group (scale bar = 20 μm). (G and H) Mean Fluorescence Intensity (MFI) of P-JAK2 and P-STAT3 proteins, detected by ImageJ. All data were normalized to the control group. Data are presented as means ± SEMs (N = 8, $^{\#\#\#\#}p < 0.0001$ compared to the control group; $^{*}p < 0.05$, $^{**}p < 0.01$, $^{***}p < 0.001$ compared to the LPS-induced group; $^{ns}p > 0.05$ compared to the LPS + EGCG 20 mg kg^{-1} group).

ment with 20 mg kg^{-1} EGCG and SCFAs reduced these levels (Fig. 12C–E). Lung tissue IF assays confirmed the suppression of JAK2/STAT3 activation (Fig. 12F and G), suggesting that EGCG and SCFAs exert anti-inflammatory effects, at least in part, by inhibiting JAK2/STAT3 signaling. In contrast, other phosphorylated proteins showed minimal involvement in the inflammatory network, with pretreatment not significantly affecting their levels (Fig. S7A–J and S8A–H). These results establish JAK2 and STAT3 play an important role in inflammatory regulation and its inhibition.

To test whether EGCG inhibits inflammation *via* SCFAs-mediated suppression, rescue experiments were conducted using the JAK2/STAT3 inhibitor WP1066 (Fig. 13A). Compared to the LPS group, the LPS + SCFAs + WP1066 group exhibited a significantly reduced level of P-JAK2 and P-STAT3 proteins in lung tissues. This reduction was notably more pronounced than in the LPS + SCFAs group (Fig. 13B–D). In BALF, the LPS + SCFAs + WP1066 group showed a significant reduction in protein levels compared to the LPS group, with the combined treatment's efficacy in reducing BALF protein levels being comparable to the LPS + EGCG group and significantly superior to the LPS + SCFAs group (Fig. 13E). Parallel improvements were observed in lung histopathology, inflammatory cell counts, and cytokine levels in serum, BALF, and lung tissue (Fig. 13F–V). Furthermore, intestinal damage was alleviated in the LPS + SCFAs + WP1066 group, achieving results similar to the LPS + EGCG group but significantly different from the LPS + SCFAs group (Fig. 14A and B). Mechanistically, colon mRNA and protein levels of ZO-1 and occludin were restored in the LPS + SCFAs + WP1066 group to levels comparable to those in the LPS + EGCG group (Fig. 14C–G). Collectively, these results suggest that SCFAs mitigate ARDS-associated inflammation and gut barrier dysfunction primarily through JAK2/STAT3 inhibition. The comparable efficacy of EGCG and SCFAs + WP1066 indicates that JAK2/STAT3 suppression is a key pathway for EGCG's anti-inflammatory action.

4. Discussion

ARDS is a severe pulmonary condition that poses a significant threat to patient health and survival.[48] The LPS-induced ARDS model is widely used in scientific research to investigate its pathogenesis and develop therapeutic strategies.[49] Tea, a globally cultivated crop known for its anti-inflammatory and antioxidant properties,[27] is a rich source of EGCG, a key natural compound that can be effectively extracted and utilized.[50] Given its therapeutic potential, EGCG offers promising prospects for ARDS treatment.[51] In the present study, the optimal dosage of EGCG was determined through a sub-acute toxicity experiment, with the safe dose set below 20 mg kg^{-1}, consistent with previous findings on the dose-safety profile of natural compounds.[52] Many such compounds exhibit toxicity at high doses, while lower doses may lack therapeutic efficacy. Identifying this optimal dose provides a safe and reliable foundation for further experiments. EGCG demonstrates notable advantages in mitigating ARDS-related inflammatory injury. Traditional ARDS treatments, such as glucocorticoids, carry significant drawbacks, including an increased risk of infection and metabolic disorders, while neuromuscular blockers may cause muscle weakness and prolonged mechanical ventilation.[4] In contrast, EGCG shows no serious toxic side effects at appropriate doses, making it suitable for long-term use or preventive applications.[26] EGCG exerts comprehensive anti-inflammatory effects at multiple biological levels. At the systemic level, it alleviates weight loss in affected mice, significantly reduces lung tissue damage, and improves histological injury scores. The compound also demonstrates potent cellular regulation, suppressing excessive inflammatory cell infiltration and modulating key protein expression, particularly reducing pro-inflammatory cytokines in serum and BALF. Additionally, EGCG precisely regulates the expression of critical inflammation-related genes, establishing its multi-target therapeutic potential against ARDS pathogenesis.[53] EGCG also shows great promise in combination therapy. It could be integrated with existing respiratory support techniques, such as lung-protective ventilation strategies and prone positioning, to enhance ARDS treatment outcomes.[54] Combining EGCG with conventional therapies may enable lower drug dosages, thereby reducing adverse effects.[26] Due to its high safety and low toxicity, EGCG may also have preventive applications. Prophylactic administration to high-risk populations, such as patients with severe infections or trauma, could potentially reduce ARDS incidence. Future research should focus on exploring EGCG's anti-inflammatory mechanisms and optimizing treatment protocols to achieve therapeutic breakthroughs in this field.

This study explored the intrinsic relationship between EGCG and gut microbiota composition within the framework of the "gut–lung axis" theory,[55] which describes the complex bidirectional interaction between intestinal microbiota and pulmonary health.[56] Existing research has shown that gut microbiota dysbiosis can impair intestinal barrier integrity, facilitating bacterial translocation that induces pulmonary immune damage and contributes to the pathogenesis of ARDS.[57] Building on this foundation, our study systematically elucidated the mechanism by which EGCG modulates gut microbiota and enhances intestinal barrier function. Comprehensive analysis of microbial communities, including α-diversity assessment and PCoA-based β-diversity evaluation, revealed distinct microbial profiles in EGCG-treated mice compared to both LPS-challenged and control groups. These differential microbiota populations suggest that EGCG exerts its therapeutic effects through targeted modulation of specific bacterial taxa. These findings are consistent with established probiotic and prebiotic research, confirming EGCG's ability to promote microbial diversity and maintain gut microecological balance. This evidence strongly supports EGCG's microbiota-regulating properties and provides key insights into its mechanism within the "gut–lung axis".[58] The present study further demonstrated that LPS-induced ARDS leads to downregulation of intestinal tight-junction proteins and barrier dysfunction,[59] while showing EGCG's ability to counteract these pathological

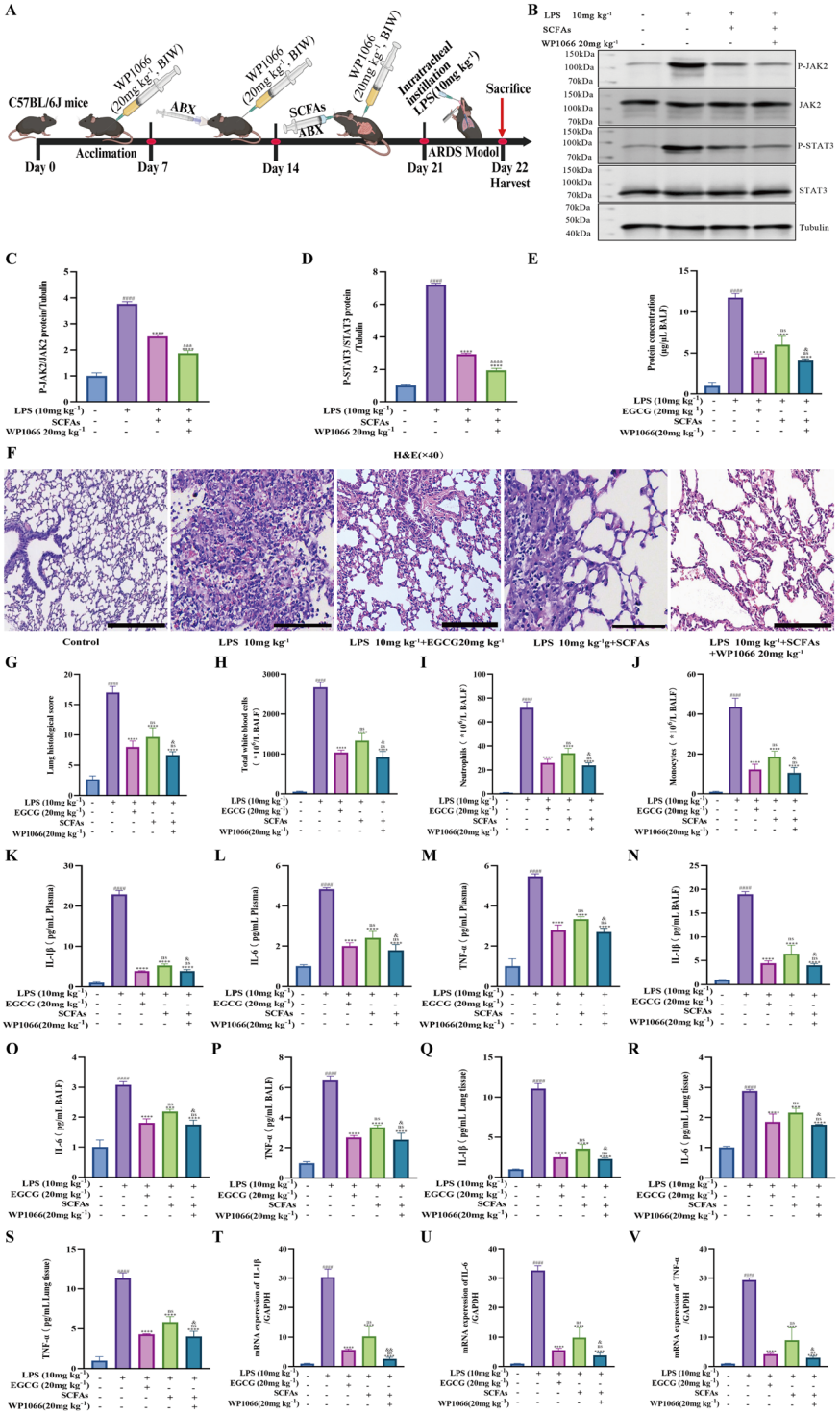

Fig. 13 SCFAs attenuate LPS-induced pulmonary inflammation in mice by inhibiting the JAK2/STAT3 signaling pathway. (A) Diagram illustrating the experimental design used in Experiment 5. (B) Protein expression levels of P-JAK2, JAK2, P-STAT3, and STAT3 in the lung tissues of mice in each group, detected by western blot analysis. (C and D) Relative protein expression levels of P-JAK2/JAK2 and P-STAT3/STAT3 to Tubulin, measured using ImageJ software. (E) Protein concentration in BALF. (F) H&E staining revealing histomorphological characteristics of the lung (scale bar = 50 μm). (G) Histological scores of lung tissues enabling quantitative analysis. (H–J) Cell count, including total white blood cells, neutrophils, and mononuclear macrophages, using a hematology analyzer. (K–M) Levels of inflammatory factors, including TNF-α, IL-6, and IL-1β, in serum, measured using ELISA kits. (N–P) Levels of inflammatory factors (TNF-α, IL-6, IL-1β) in BALF, measured using ELISA kits. (Q–S) Levels of inflammatory factors (TNF-α, IL-6, IL-1β) in lung tissues, measured using ELISA kits. (T–V) RT-PCR analysis of inflammatory factors (TNF-α, IL-6, IL-1β) in lung tissues. All data were normalized to the control group. Data are presented as means ± SEMs (N = 8, $^{\#\#\#}p < 0.001$, $^{\#\#\#\#}p < 0.0001$ compared to the control group; $^{****}p < 0.0001$ compared to the LPS-induced group; $^{ns}p > 0.05$ compared to the LPS + EGCG 20 mg kg^{-1} group; $^{\&}p < 0.05$, $^{\&\&}p < 0.01$, $^{\&\&\&}p < 0.001$, $^{\&\&\&\&}p < 0.0001$ compared to the LPS + SCFAs group).

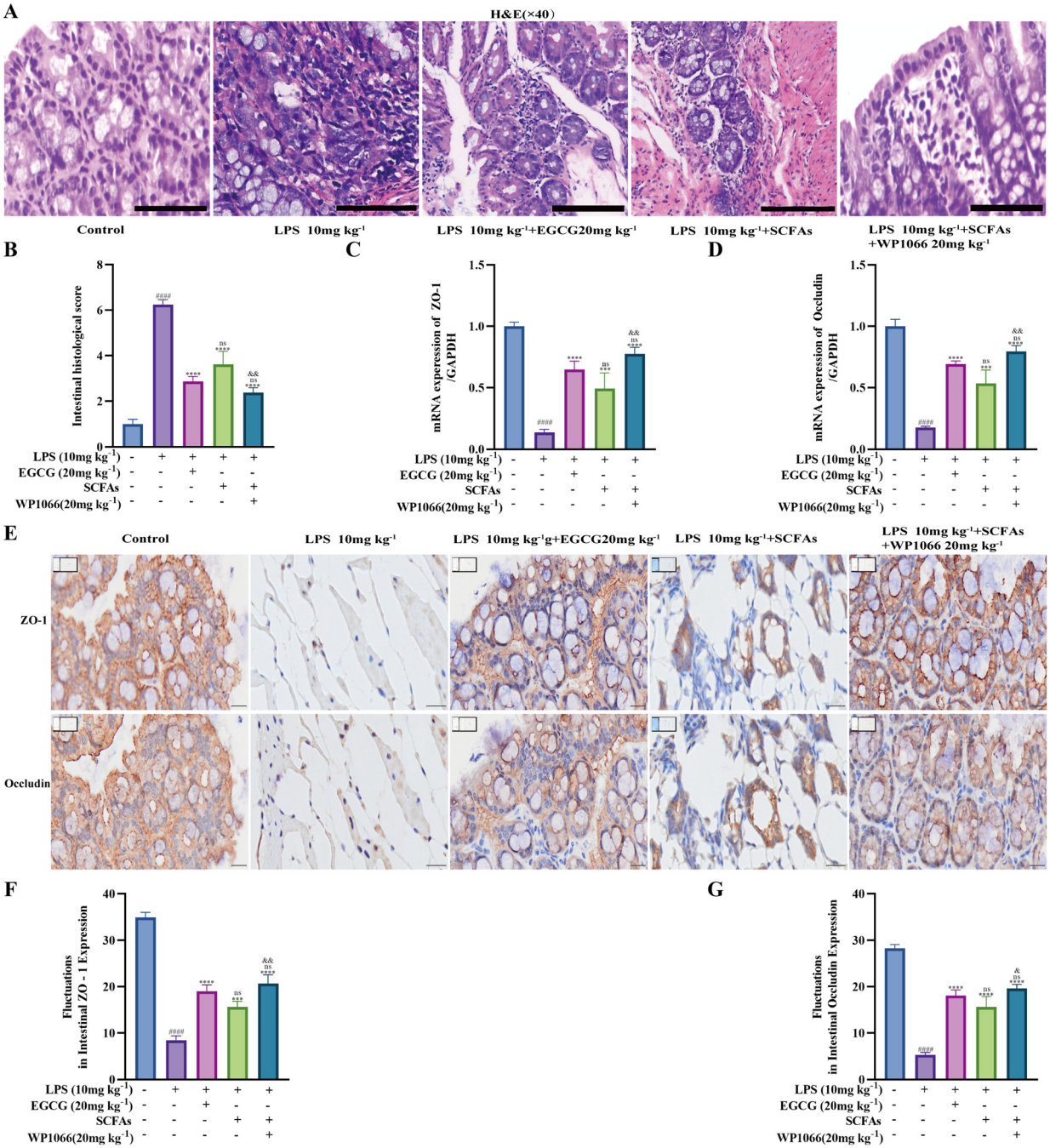

Fig. 14 SCFAs alleviate LPS-induced intestinal mucosal injury in mice by regulating the JAK2/STAT3 signaling pathway. (A) H&E staining of intestinal tissues from each group of mice (scale bar = 50 μm). (B) Quantitative analysis of histological scores of intestinal tissues. (C and D) RT-PCR analysis of ZO-1 and occludin levels in mouse intestinal tissues. (E) Immunohistochemical detection of ZO-1 and occludin protein expression in intestinal tissues (scale bar = 20 μm). (F and G) Mean Fluorescence Intensity (MFI) of ZO-1 and occludin proteins, measured by ImageJ. All data were normalized to the control group. Data are presented as means ± SEMs (N = 8, $^{\#\#\#\#}p < 0.0001$ compared to the control group; $^{*}p < 0.05$, $^{**}p < 0.01$, $^{***}p < 0.001$ compared to the LPS-induced group; $^{ns}p > 0.05$ compared to the LPS + EGCG 20 mg kg^{-1} group; $^{\&}p < 0.05$, $^{\&\&}p < 0.01$ compared to the LPS + SCFAs group).

changes. This protective effect on gut barrier integrity establishes a novel theoretical framework for EGCG's therapeutic application in ARDS. Unlike conventional approaches that focus on EGCG's direct pulmonary anti-inflammatory effects,[60,61] our research highlights its indirect mechanism through gut microbiota regulation and barrier enhancement. Notably, EGCG treatment significantly increased the relative abundance of beneficial bacteria, such as AKK, suggesting its potential to influence pulmonary health *via* gut-mediated pathways. This hypothesis was conclusively validated through

innovative FMT experiments, which showed that EGCG-modulated gut microbiota alone could attenuate ARDS inflammation without direct pulmonary intervention. Recipient mice exhibited restored tight-junction protein expression and ameliorated intestinal inflammation, providing definitive evidence that gut barrier improvement can mitigate pulmonary infection and inflammation. These findings significantly advance our understanding of gut–lung axis interactions and position EGCG as a promising therapeutic candidate for ARDS, acting through its dual action on gut microbiota composition and barrier function. The FMT results particularly highlight the potential of microbiota-targeted interventions in respiratory disease management.

This study provides a systematic and mechanistic understanding of how EGCG intervention modulates the relative abundance of AKK to alleviate ARDS-related inflammatory damage, marking a significant advancement beyond previous findings. While earlier studies have established a general connection between gut microbiota imbalance and pulmonary inflammation, as well as broad correlations between microbial community changes and respiratory infections,[62,63] our work specifically identifies AKK as a key microbial mediator in this process. Rigorous experimental validation demonstrated that EGCG-induced increases in AKK relative abundance directly correlate with therapeutic improvements, and that transplantation of this specific bacterium alone can effectively mitigate LPS-induced ARDS pathology. These findings provide concrete evidence supporting the application of the "gut–lung axis" theory in ARDS research. This study presents several important advancements over prior research. Previous studies examining the effects of probiotics on pulmonary inflammation[64] lacked the specificity of our work, which not only confirms AKK's anti-inflammatory properties but also elucidates its shared mechanistic pathways with EGCG. This represents a more refined understanding of microbial-host interactions in inflammatory lung diseases. Furthermore, while traditional ARDS treatment research has primarily focused on pulmonary-targeted pharmaceuticals and mechanical ventilation,[65] with most natural product studies overlooking the role of gut microbiota,[65,66] our discovery of EGCG's action through AKK modulation introduces a novel therapeutic approach. Notably, this study bridges a critical gap in existing research by demonstrating AKK's dual capacity to both reduce inflammation and repair intestinal barrier damage,[8] underscoring the essential role of gut homeostasis in comprehensive ARDS management. Collectively, these findings establish gut microbiota modulation as a promising new strategy for ARDS treatment, offering specific mechanistic insights that could guide future therapeutic development.

This study elucidates the therapeutic potential of EGCG in ARDS through a comprehensive investigation of its gut microbiota-mediated mechanisms. Metabolomic analysis revealed that SCFAs represent the most significantly altered gut metabolites during AKK-mediated intervention, consistent with previous reports.[38,67] As essential microbial metabolites, SCFAs play pivotal roles in host physiological processes, including immune regulation and energy metabolism.[68] They exhibit potent anti-inflammatory effects by precisely modulating immune cell functions and signaling pathways.[24,69] Experimental validation demonstrated that SCFAs alone can mitigate LPS-induced ARDS inflammatory injury, with efficacy comparable to EGCG. This suggests that EGCG may exert its therapeutic effects by enhancing AKK relative abundance, thereby elevating SCFAs levels. Compared to conventional ARDS anti-inflammatory treatments, such as glucocorticoids and NSAIDs, which directly target inflammatory pathways and often lead to adverse effects like immunosuppression and metabolic disturbances,[70] EGCG's microbiota-modulating approach offers distinct advantages. Mechanistic studies employing various experimental approaches identified that EGCG's anti-inflammatory action involves SCFAs-mediated inhibition of JAK2/STAT3 phosphorylation and activation. While the JAK2/STAT3 pathway is implicated in several diseases, including IBD and metabolic syndrome, its regulation through SCFAs in ARDS represents a unique anti-inflammatory mechanism, consistent with established views on this pathway's role in inflammation control.[71,72]

This study has several limitations. Although the involvement of the AKK-SCFAs-JAK2/STAT3 axis in EGCG's therapeutic effects has been established, several mechanistic details remain unclear. First, the precise mechanism by which EGCG regulates the relative abundance of AKK is not fully understood, though existing studies have explored potential pathways. For example, EGCG has been shown to increase AKK abundance by altering gut microbiome composition and inhibiting the growth of competitive microorganisms.[38] Specifically, EGCG may reduce the population of bacteria that hinder AKK growth by influencing bile acid composition, thereby creating a favorable environment for AKK proliferation.[73] Moreover, EGCG's antibacterial properties may reduce competitive pressure on AKK, indirectly promoting its growth.[30] Further research suggests that EGCG could serve as a nutrient source to support AKK growth, influence the gut metabolic environment, and potentially increase AKK abundance by activating the Takeda G protein-coupled receptor (TGR-5), which regulates metabolic signaling pathways.[74] Second, the specific mechanism by which AKK regulates the production of SCFAs remains unclear. Currently, this study has only confirmed that AKK can affect SCFAs levels; however, in-depth investigation into the core mechanism by which AKK regulates gut microbiota metabolism and promotes the synthesis and secretion of SCFAs has not been conducted, which requires further clarification in subsequent experiments. Third, the specific transport mechanisms by which SCFAs reach pulmonary tissues remain unclear. It is speculated that SCFAs may rely on transport proteins such as monocarboxylate transporters (MCTs) or enter lung cells through passive diffusion.[75] The concentration and distribution of SCFAs in the blood, as well as their binding to plasma proteins, could affect their transport efficiency.[76] Furthermore, SCFAs exhibit biological activity in the lungs, activating G protein-coupled receptors, modulating immune and inflammatory responses,

and promoting their own accumulation and functional exertion.[77] Consequently, it must be emphasized that we evaluated only the prophylactic efficacy of EGCG administered before LPS challenge; the model does not encompass post-LPS administration, so our conclusions are restricted to blockade of the initiating phase and cannot be extended to therapeutic applications. Future studies should establish post-LPS or repeated-dosing protocols to directly examine EGCG's therapeutic window and dose–effect relationship. While the animal-based findings provide strong preclinical evidence, rigorous clinical studies are required to validate their translational potential for human ARDS treatment.

5. Conclusion

This study reveals a novel gut–lung axis mechanism through which EGCG exerts its therapeutic effects in LPS-induced ARDS. EGCG treatment specifically enriches AKK in the gut microbiota, leading to increased production of SCFAs. These microbial metabolites are absorbed into systemic circulation and transported to the lungs, where they attenuate inflammatory responses by modulating the JAK2/STAT3 signaling pathway. This provides the first experimental evidence for a gut microbiota-dependent mechanism of EGCG in ARDS treatment, establishing a critical link between intestinal microbial metabolites and pulmonary inflammation resolution. The discovery of the AKK-SCFAs-JAK2/STAT3 axis not only offers new therapeutic possibilities for ARDS management but also enhances our understanding of gut-derived metabolite regulation in inflammatory lung diseases, potentially informing treatment strategies for other inflammation-related conditions.

Authors' contributions

Conceptualization, data curation, formal analysis, funding acquisition, investigation, visualization, and the original draft were carried out by Shiming Fan, Xianming Fan, Yan Ren, and Guofang Yin. Supervision, validation, and project administration were handled by Xianming Fan and Dan Luo. Additional financial support was obtained by Xiaoqing Fan, Yuling Liang, Ning Ma, Ying Luo, Yi Deng, Chunmei Zhang, Tian Xiang, Jing Zuo, and Jingli Tang.

Ethics approval and consent to participate

The animal study was reviewed and approved by the Animal Ethics Committee (AEC) of Southwest Medical University.

Conflicts of interest

The authors declare that they have no competing interests.

Data availability

All data supporting the findings of this study, including raw qRT-PCR, ELISA, western blot, histopathology (H&E), immunofluorescence, immunohistochemistry, 16S rRNA sequencing, metabolomics, network pharmacology, and transcriptomics data, as well as anonymized survival analysis data and analysis code, have been deposited in the Figshare repository and are publicly available under https://doi.org/10.6084/m9.figshare.29664380, https://doi.org/10.6084/m9.figshare.30996073, and https://doi.org/10.6084/m9.figshare.29664416. Any additional materials are available from the corresponding author upon reasonable request.

Supplementary information (SI) is available. See DOI: https://doi.org/10.1039/d5fo05380c.

Acknowledgements

This investigation was financially supported by the Yibin Science and Technology program (Grant No. 2023SF002), the Jiang'an County Bureau of Economic Commerce, Informatization, and Science and Technology (Grant No. 2023SF01), the Natural Science Foundation of Sichuan province (No. 2022NSFSC0046), the Sichuan Science and Technology program (No. 2022YFS0631), the Luzhou Science and Technology program (No. 2023JYJ049), the School-level Scientific Research project of Southwestern Medical University (No. 2023ZD007), the University Sponsored Research Program of Southwest Medical University (No. 2025LCYXZX39).

This study acknowledges the significant technical support and resource provision from Southwest Medical University's Advanced Precision Instrument platform, Cellular and Molecular platform, and Animal Center. These platforms provided essential assistance in equipment use, experimental operations, and data analysis, forming a solid foundation for the smooth implementation and successful completion of the research.

References

1 K. D. Wick, L. B. Ware and M. A. Matthay, Acute respiratory distress syndrome, *Br. Med. J.*, 2024, **387**, e076612, DOI: 10.1136/bmj-2023-076612.
2 P. Yang and M. W. Sjoding, Acute Respiratory Distress Syndrome: Definition, Diagnosis, and Routine Management, *Crit. Care Clin.*, 2024, **40**, 309–327, DOI: 10.1016/j.ccc.2023.12.003.
3 D. Jayasimhan and M. A. Matthay, Definitions of Acute Respiratory Distress Syndrome: Present Recommendations and Challenges, *Clin. Chest Med.*, 2024, **45**, 785–795, DOI: 10.1016/j.ccm.2024.08.001.
4 C. Pan, L. Liu, J. F. Xie and H. B. Qiu, Acute Respiratory Distress Syndrome: Challenge for Diagnosis and Therapy,

Chin. Med. J., 2018, **131**, 1220–1224, DOI: 10.4103/0366-6999.228765.

5 J. R. Beitler, *et al.*, Advancing precision medicine for acute respiratory distress syndrome, *Lancet Respir. Med.*, 2022, **10**, 107–120, DOI: 10.1016/s2213-2600(21)00157-0.

6 Y. Xu, *et al.*, Akkermansia muciniphila Alleviates Persistent Inflammation, Immunosuppression, and Catabolism Syndrome in Mice, *Metabolites*, 2023, **13**(2), 194, DOI: 10.3390/metabo13020194.

7 J. Shen, *et al.*, Akkermansia muciniphila attenuated lipopolysaccharide-induced acute lung injury by modulating the gut microbiota and SCFAs in mice, *Food Funct.*, 2023, **14**, 10401–10417, DOI: 10.1039/d3fo04051h.

8 S. Xiong, *et al.*, Kuqin ameliorates Lipopolysaccharide-induced acute lung injury by regulating indoleamine 2,3-dioxygenase 1 and Akkermansia muciniphila, *Biomed. Pharmacother.*, 2023, **158**, 114073, DOI: 10.1016/j.biopha.2022.114073.

9 Y. He, *et al.*, Imbalance of intestinal flora activates inflammatory response contributing to acute lung injury, *J. Thorac. Dis.*, 2024, **16**, 6835–6848, DOI: 10.21037/jtd-24-633.

10 L. Tang, *et al.*, Unlocking the potential of Rosa roxburghii Tratt polyphenol: a novel approach to treating acute lung injury from a perspective of the lung-gut axis, *Front. Microbiol.*, 2024, **15**, 1351295, DOI: 10.3389/fmicb.2024.1351295.

11 C. Grajeda-Iglesias, *et al.*, Oral administration of Akkermansia muciniphila elevates systemic antiaging and anticancer metabolites, *Aging*, 2021, **13**, 6375–6405, DOI: 10.18632/aging.202739.

12 A. Mohammed, *et al.*, Protective effects of Δ(9) -tetrahydrocannabinol against enterotoxin-induced acute respiratory distress syndrome are mediated by modulation of microbiota, *Br. J. Pharmacol.*, 2020, **177**, 5078–5095, DOI: 10.1111/bph.15226.

13 Q. Ge, *et al.*, In vitro fermentation characteristics of polysaccharides from coix seed and its effects on the gut microbiota, *Int. J. Biol. Macromol.*, 2024, **262**, 129994, DOI: 10.1016/j.ijbiomac.2024.129994.

14 Z. Wang, *et al.*, The gut-lung axis in severe acute Pancreatitis-associated lung injury: The protection by the gut microbiota through short-chain fatty acids, *Pharmacol. Res.*, 2022, **182**, 106321, DOI: 10.1016/j.phrs.2022.106321.

15 R. Tang, *et al.*, Huoxiang Zhengqi Oral Liquid Attenuates LPS-Induced Acute Lung Injury by Modulating Short-Chain Fatty Acid Levels and TLR4/NF-κB p65 Pathway, *BioMed. Res. Int.*, 2023, **2023**, 6183551, DOI: 10.1155/2023/6183551.

16 Z. Wang, *et al.*, Mechanisms of Qingyi Decoction in Severe Acute Pancreatitis-Associated Acute Lung Injury via Gut Microbiota: Targeting the Short-Chain Fatty Acids-Mediated AMPK/NF-κB/NLRP3 Pathway, *Microbiol. Spectrum*, 2023, **11**, e0366422, DOI: 10.1128/spectrum.03664-22.

17 D. S. Finbloom and A. C. Larner, Regulation of the Jak/STAT signalling pathway, *Cell. Signalling*, 1995, **7**, 739–745, DOI: 10.1016/0898-6568(95)02004-7.

18 S. B. Wang and Y. M. Yao, Advances in basic research on Janus kinase/signal transducer and activators of transcription pathway and sepsis, *Zhongguo Weizhongbing Jijiu Yixue*, 2003, **15**, 690–693.

19 F. Cao, *et al.*, Suppression of NLRP3 Inflammasome by Erythropoietin via the EPOR/JAK2/STAT3 Pathway Contributes to Attenuation of Acute Lung Injury in Mice, *Front. Pharmacol.*, 2020, **11**, 306, DOI: 10.3389/fphar.2020.00306.

20 J. Zhou, P. Zhou, Y. Zhang, G. Wang and Z. Fan, Signal Pathways and Markers Involved in Acute Lung Injury Induced by Acute Pancreatitis, *Dis. Markers*, 2021, 9947047, DOI: 10.1155/2021/9947047.

21 O. M. Al-Fakhrany and E. Elekhnawy, Next-generation probiotics: the upcoming biotherapeutics, *Mol. Biol. Rep.*, 2024, **51**, 505, DOI: 10.1007/s11033-024-09398-5.

22 H. Liu, *et al.*, Live Akkermansia muciniphila boosts dendritic cell retinoic acid synthesis to modulate IL-22 activity and mitigate colitis in mice, *Microbiome*, 2024, **12**, 275, DOI: 10.1186/s40168-024-01995-7.

23 S. Yang, *et al.*, Xiaoyankangjun tablet alleviates dextran sulfate sodium-induced colitis in mice by regulating gut microbiota and JAK2/STAT3 pathway, *Nat. Prod. Bioprospect.*, 2024, **14**, 44, DOI: 10.1007/s13659-024-00468-6.

24 M. Li, *et al.*, Pro- and anti-inflammatory effects of short chain fatty acids on immune and endothelial cells, *Eur. J. Pharmacol.*, 2018, **831**, 52–59, DOI: 10.1016/j.ejphar.2018.05.003.

25 X. Tang, *et al.*, Butyric Acid Increases the Therapeutic Effect of EHLJ7 on Ulcerative Colitis by Inhibiting JAK2/STAT3/SOCS1 Signaling Pathway, *Front. Pharmacol.*, 2019, **10**, 1553, DOI: 10.3389/fphar.2019.01553.

26 B. N. Singh, S. Shankar and R. K. Srivastava, Green tea catechin, epigallocatechin-3-gallate (EGCG): mechanisms, perspectives and clinical applications, *Biochem. Pharmacol.*, 2011, **82**, 1807–1821, DOI: 10.1016/j.bcp.2011.07.093.

27 T. Ohishi, S. Goto, P. Monira, M. Isemura and Y. Nakamura, Anti-inflammatory Action of Green Tea, *Antiinflamm. Antiallergy Agents Med. Chem.*, 2016, **15**, 74–90, DOI: 10.2174/1871523015666160915154443.

28 J. Wang, S. M. Fan and J. Zhang, Epigallocatechin-3-gallate ameliorates lipopolysaccharide-induced acute lung injury by suppression of TLR4/NF-κB signaling activation, *Braz. J. Med. Biol. Res.*, 2019, **52**, e8092, DOI: 10.1590/1414-431x20198092.

29 J. Wang, *et al.*, Therapeutic Effects and Molecular Mechanisms of Bioactive Compounds Against Respiratory Diseases: Traditional Chinese Medicine Theory and High-Frequency Use, *Front. Pharmacol.*, 2021, **12**, 734450, DOI: 10.3389/fphar.2021.734450.

30 L. Sheng, *et al.*, Obesity treatment by epigallocatechin-3-gallate-regulated bile acid signaling and its enriched Akkermansia muciniphila, *FASEB J.*, 2018, **32**, fj201800370R, DOI: 10.1096/fj.201800370R.

31 H. W. Jeong, *et al.*, Green Tea Encourages Growth of Akkermansia muciniphila, *J. Med. Food*, 2020, **23**, 841–851, DOI: 10.1089/jmf.2019.4662.

32 Z. Liu, W. J. C. de Bruijn, M. E. Bruins and J. P. Vincken, Reciprocal Interactions between Epigallocatechin-3-gallate (EGCG), and Human Gut Microbiota In Vitro, *J. Agric. Food Chem.*, 2020, **68**, 9804–9815, DOI: 10.1021/acs.jafc.0c03587.
33 X. Xiao, *et al.*, (-)-Epigallocatechin-3-gallate induces cell apoptosis in chronic myeloid leukaemia by regulating Bcr/Abl-mediated p38-MAPK/JNK and JAK2/STAT3/AKT signalling pathways, *Clin. Exp. Pharmacol. Physiol.*, 2019, **46**, 126–136, DOI: 10.1111/1440-1681.13037.
34 L. Mao, *et al.*, Green Tea Polyphenol (-)-Epigallocatechin Gallate (EGCG) Attenuates Neuroinflammation in Palmitic Acid-Stimulated BV-2 Microglia and High-Fat Diet-Induced Obese Mice, *Int. J. Mol. Sci.*, 2019, **20**(20), 5081, DOI: 10.3390/ijms20205081.
35 X. Fan, *et al.*, Herbal formula BaWeiBaiDuSan alleviates polymicrobial sepsis-induced liver injury via increasing the gut microbiota Lactobacillus johnsonii and regulating macrophage anti-inflammatory activity in mice, *Acta Pharm. Sin. B*, 2023, **13**, 1164–1179, DOI: 10.1016/j.apsb.2022.10.016.
36 J. Tang, L. Xu, Y. Zeng and F. Gong, Effect of gut microbiota on LPS-induced acute lung injury by regulating the TLR4/NF-kB signaling pathway, *Int. Immunopharmacol.*, 2021, **91**, 107272, DOI: 10.1016/j.intimp.2020.107272.
37 S. Fan, Y. Ren, W. Zhang, H. Zhang and C. Wang, Long non-coding maternally expressed gene 3 regulates cigarette smoke extract-induced apoptosis, inflammation and cytotoxicity by sponging miR-181a-2–3p in 16HBE cells, *Oncol. Lett.*, 2021, **21**, 45, DOI: 10.3892/ol.2020.12306.
38 Z. Wu, *et al.*, Gut microbiota from green tea polyphenol-dosed mice improves intestinal epithelial homeostasis and ameliorates experimental colitis, *Microbiome*, 2021, **9**, 184, DOI: 10.1186/s40168-021-01115-9.
39 P. S. Seethalakshmi, *et al.*, Comparative analysis of commercially available kits for optimal DNA extraction from bovine fecal samples, *Arch. Microbiol.*, 2024, **206**, 314, DOI: 10.1007/s00203-024-04047-8.
40 J. Jia, *et al.*, Inhibition of METTL3 alleviated LPS-induced alveolar epithelial cell apoptosis and acute lung injury via restoring neprilysin expression, *Life Sci.*, 2023, **333**, 122148, DOI: 10.1016/j.lfs.2023.122148.
41 C. Yang, *et al.*, Re-Du-Ning injection ameliorates LPS-induced lung injury through inhibiting neutrophil extracellular traps formation, *Phytomedicine*, 2021, **90**, 153635, DOI: 10.1016/j.phymed.2021.153635.
42 J. Fu, *et al.*, In-depth investigation of the mechanisms of Schisandra chinensis polysaccharide mitigating Alzheimer's disease rat via gut microbiota and feces metabolomics, *Int. J. Biol. Macromol.*, 2023, **232**, 123488, DOI: 10.1016/j.ijbiomac.2023.123488.
43 W. Hu, Z. Wu, M. Zhang, S. Yu and X. Zou, Identification of ferroptosis-related genes in male mice with sepsis-induced acute lung injury based on transcriptome sequencing, *BMC Pulm. Med.*, 2023, **23**, 133, DOI: 10.1186/s12890-023-02361-3.
44 J. J. Wen, *et al.*, Tea polyphenol and epigallocatechin gallate ameliorate hyperlipidemia via regulating liver metabolism and remodeling gut microbiota, *Food Chem.*, 2023, **404**, 134591, DOI: 10.1016/j.foodchem.2022.134591.
45 W. Song, *et al.*, Sinomenine ameliorates septic acute lung injury in mice by modulating gut homeostasis via aryl hydrocarbon receptor/Nrf2 pathway, *Eur. J. Pharmacol.*, 2021, **912**, 174581, DOI: 10.1016/j.ejphar.2021.174581.
46 G. Zuo, *et al.*, Tea Polyphenol Epigallocatechin Gallate Protects Against Nonalcoholic Fatty Liver Disease and Associated Endotoxemia in Rats via Modulating Gut Microbiota Dysbiosis and Alleviating Intestinal Barrier Dysfunction and Related Inflammation, *J. Agric. Food Chem.*, 2024, 12, DOI: 10.1021/acs.jafc.3c04832.
47 S. Ferrari, R. Galla, S. Mulè and F. Uberti, Analysis of the Beneficial Effects of Probiotics on the Gut-Prostate Axis Using Prostatic Co-Culture Model, *Foods*, 2024, **16**, 3647, DOI: 10.3390/foods13223647.
48 E. Fan, D. Brodie and A. S. Slutsky, Acute Respiratory Distress Syndrome: Advances in Diagnosis and Treatment, *J. Am. Med. Assoc.*, 2018, **319**, 698–710, DOI: 10.1001/jama.2017.21907.
49 H. Chen, C. Bai and X. Wang, The value of the lipopolysaccharide-induced acute lung injury model in respiratory medicine, *Expert Rev. Respir. Med.*, 2010, **4**, 773–783, DOI: 10.1586/ers.10.71.
50 S. Zhang, *et al.*, Absorption, metabolism, bioactivity, and biotransformation of epigallocatechin gallate, *Crit. Rev. Food Sci. Nutr.*, 2024, **64**, 6546–6566, DOI: 10.1080/10408398.2023.2170972.
51 K. I. Tanaka, *et al.*, Preventive Effect of Epigallocatechin Gallate, the Main Component of Green Tea, on Acute Lung Injury Caused by Air Pollutants, *Biomolecules*, 2022, **12**, 1196, DOI: 10.3390/biom12091196.
52 M. K. Cheung, G. G. L. Yue, P. W. Y. Chiu and C. B. S. Lau, A Review of the Effects of Natural Compounds, Medicinal Plants, and Mushrooms on the Gut Microbiota in Colitis and Cancer, *Front. Pharmacol.*, 2020, **11**, 744, DOI: 10.3389/fphar.2020.00744.
53 J. H. Azambuja, R. I. Mancuso, F. I. D. Via, C. O. Torello and S. T. O. Saad, Protective effect of green tea and epigallocatechin-3-gallate in a LPS-induced systemic inflammation model, *J. Nutr. Biochem.*, 2022, **101**, 108920, DOI: 10.1016/j.jnutbio.2021.108920.
54 B. Kasper, *et al.*, Epigallocatechin gallate attenuates cardiopulmonary bypass-associated lung injury, *J. Surg. Res.*, 2016, **201**, 313–325, DOI: 10.1016/j.jss.2015.11.007.
55 K. F. Budden, *et al.*, Emerging pathogenic links between microbiota and the gut-lung axis, *Nat. Rev. Microbiol.*, 2017, **15**, 55–63, DOI: 10.1038/nrmicro.2016.142.
56 M. W. Adelman, *et al.*, The gut microbiome's role in the development, maintenance, and outcomes of sepsis, *Crit. Care*, 2020, **24**, 278, DOI: 10.1186/s13054-020-02989-1.
57 Q. He, *et al.*, Herbal medicine in the treatment of COVID-19 based on the gut-lung axis, *Acupunct. Herb. Med.*, 2022, **2**, 172–183, DOI: 10.1097/hm9.0000000000000038.
58 F. F. Khan, *et al.*, Recent Innovations in Non-dairy Prebiotics and Probiotics: Physiological Potential, Applications, and

Characterization, *Probiotics Antimicrob. Proteins*, 2023, **15**, 239–263, DOI: 10.1007/s12602-022-09983-9.

59 S. Cai, *et al.*, (-)-Epigallocatechin-3-Gallate (EGCG) Modulates the Composition of the Gut Microbiota to Protect Against Radiation-Induced Intestinal Injury in Mice, *Front. Oncol.*, 2022, **12**, 848107, DOI: 10.3389/fonc.2022.848107.

60 X. Zhang, F. He, J. Yang and Z. S. Chen, Protective effects of epigallocatechin-3-gallate on intestinal ischemia reperfusion injury through enhanced activation of PI3K/Akt pathway in rats, *J. Huazhong Univ. Sci. Technol., Med. Sci.*, 2015, **35**, 378–383, DOI: 10.1007/s11596-015-1441-2.

61 H. B. Bae, *et al.*, The effect of epigallocatechin gallate on lipopolysaccharide-induced acute lung injury in a murine model, *Inflammation*, 2010, **33**, 82–91, DOI: 10.1007/s10753-009-9161-z.

62 Y. Ma, G. Liu, M. Tang, J. Fang and H. Jiang, Epigallocatechin Gallate Can Protect Mice From Acute Stress Induced by LPS While Stabilizing Gut Microbes and Serum Metabolites Levels, *Front. Immunol.*, 2021, **12**, 640305, DOI: 10.3389/fimmu.2021.640305.

63 Z. Ren, Z. Zheng and X. Feng, Role of gut microbes in acute lung injury/acute respiratory distress syndrome, *Gut Microbes*, 2024, **16**, 2440125, DOI: 10.1080/19490976.2024.2440125.

64 S. Nasreen, *et al.*, Mechanisms of medicinal, pharmaceutical, and immunomodulatory action of probiotics bacteria and their secondary metabolites against disease management: an overview, *Folia Microbiol.*, 2024, **69**, 549–565, DOI: 10.1007/s12223-024-01155-2.

65 H. Yadav, B. T. Thompson and O. Gajic, Fifty Years of Research in ARDS. Is Acute Respiratory Distress Syndrome a Preventable Disease?, *Am. J. Respir. Crit. Care Med.*, 2017, **195**, 725–736, DOI: 10.1164/rccm.201609-1767CI.

66 Y. Q. He, *et al.*, Natural product derived phytochemicals in managing acute lung injury by multiple mechanisms, *Pharmacol. Res.*, 2021, **163**, 105224, DOI: 10.1016/j.phrs.2020.105224.

67 M. Shi, E. Watson, M. Conlon, L. Sanguansri and M. A. Augustin, Impact of Co-Delivery of EGCG and Tuna Oil within a Broccoli Matrix on Human Gut Microbiota, Phenolic Metabolites and Short Chain Fatty Acids In Vitro, *Molecules*, 2022, **27**, 656, DOI: 10.3390/molecules27030656.

68 E. S. Chambers, D. J. Morrison and G. Frost, Control of appetite and energy intake by SCFA: what are the potential underlying mechanisms?, *Proc. Nutr. Soc.*, 2015, **74**, 328–336, DOI: 10.1017/s0029665114001657.

69 A. Koh, F. De Vadder, P. Kovatcheva-Datchary and F. Bäckhed, From Dietary Fiber to Host Physiology: Short-Chain Fatty Acids as Key Bacterial Metabolites, *Cell*, 2016, **165**, 1332–1345, DOI: 10.1016/j.cell.2016.05.041.

70 H. Banavasi, P. Nguyen, H. Osman and A. O. Soubani, Management of ARDS - What Works and What Does Not, *Am. J. Med. Sci.*, 2021, **362**, 13–23, DOI: 10.1016/j.amjms.2020.12.019.

71 L. Qi, *et al.*, Mechanism of Qingdai in Alleviating Acute Lung Injury by Inhibiting the JAK2/STAT3 Signaling Pathway, *J. Inflamm. Res.*, 2024, **17**, 11403–11417, DOI: 10.2147/jir.S498299.

72 B. K. Gajjela and M. M. Zhou, Calming the cytokine storm of COVID-19 through inhibition of JAK2/STAT3 signaling, *Drug Discovery Today*, 2022, **27**, 390–400, DOI: 10.1016/j.drudis.2021.10.016.

73 C. Ushiroda, *et al.*, Green tea polyphenol (epigallocatechin-3-gallate) improves gut dysbiosis and serum bile acids dysregulation in high-fat diet-fed mice, *J. Clin. Biochem. Nutr.*, 2019, **65**, 34–46, DOI: 10.3164/jcbn.18-116.

74 Y. Xia, *et al.*, In vitro co-metabolism of epigallocatechin-3-gallate (EGCG) by the mucin-degrading bacterium Akkermansia muciniphila, *PLoS One*, 2021, **16**, e0260757, DOI: 10.1371/journal.pone.0260757.

75 J. R. Han, *et al.*, Improving the in vitro and in vivo bioavailability of pterostilbene using Yesso scallop gonad protein isolates-epigallocatechin gallate (EGCG) conjugate-based emulsions: effects of carrier oil, *Food Funct.*, 2022, **13**, 9544–9558, DOI: 10.1039/d2fo01648f.

76 M. Nakatani, R. Inoue, S. Tomonaga, K. Fukuta and T. Tsukahara, Production, Absorption, and Blood Flow Dynamics of Short-Chain Fatty Acids Produced by Fermentation in Piglet Hindgut during the Suckling¯Weaning Period, *Nutrients*, 2018, **10**, DOI: 10.3390/nu10091220.

77 C. Liu, *et al.*, Immunomodulatory roles of butyrate in asthma: mechanisms and therapeutic potentials, *Front. Immunol.*, 2025, **16**, 1639606, DOI: 10.3389/fimmu.2025.1639606.